

Mn(III) complexes with nitro-substituted ligands—Spin states with a twist

Cite as: J. Appl. Phys. **129**, 213903 (2021); <https://doi.org/10.1063/5.0050276>

Submitted: 13 March 2021 . Accepted: 10 May 2021 . Published Online: 04 June 2021

 Irina A. Kühne, Laurence C. Gavin, Michelle Harris, Brendan Gildea, Helge Müller-Bunz,  Matthias Stein, and  Grace G. Morgan

COLLECTIONS

Paper published as part of the special topic on [Spin Transition Materials: Molecular and Solid-State](#)



View Online



Export Citation



CrossMark

ARTICLES YOU MAY BE INTERESTED IN

Magnetism in curved geometries

Journal of Applied Physics **129**, 210902 (2021); <https://doi.org/10.1063/5.0054025>

Special optical performance from single upconverting micro/nanoparticles

Journal of Applied Physics **129**, 210901 (2021); <https://doi.org/10.1063/5.0052876>

Magneto-optical methods for magnetoplasmonics in noble metal nanostructures

Journal of Applied Physics **129**, 211101 (2021); <https://doi.org/10.1063/5.0050034>



Webinar
How to Characterize Magnetic Materials Using Lock-in Amplifiers




[Register now](#)

Mn(III) complexes with nitro-substituted ligands—Spin states with a twist

Cite as: J. Appl. Phys. 129, 213903 (2021); doi: 10.1063/5.0050276

Submitted: 13 March 2021 · Accepted: 10 May 2021 ·

Published Online: 4 June 2021



View Online



Export Citation



CrossMark

Irina A. Kühne,^{1,2}  Laurence C. Gavin,¹ Michelle Harris,¹ Brendan Gildea,¹ Helge Müller-Bunz,¹ Matthias Stein,^{3,a)}  and Grace G. Morgan^{1,a)} 

AFFILIATIONS

¹School of Chemistry, University College Dublin (UCD), Belfield, Dublin 4, Ireland

²FZU-Institute of Physics-Czech Academy of Sciences, Na Slovance 1999/2, 182 21 Prague 8, Czech Republic

³Max Planck Institute for Dynamics of Complex Technical Systems, Molecular Simulations and Design Group, Sandtorstrasse 1, 39106 Magdeburg, Germany

Note: This paper is part of the Special Topic on Spin Transition Materials: Molecular and Solid-State.

a) Authors to whom correspondence should be addressed: matthias.stein@mpi-magdeburg.mpg.de and grace.morgan@ucd.ie

ABSTRACT

Structural, magnetic, and computational data on two new Mn(III) complex cations in lattices with five different counterions and varying levels of solvation are compared to investigate the influence of the position of the electron-withdrawing ligand nitro-substituent on the thermal spin crossover profile. The $[\text{MnL}_1]^+$ (a) and $[\text{MnL}_2]^+$ (b) complex cations were prepared by complexation of Mn(III) to the Schiff base chelates formed from condensation of 3-nitrosalicylaldehyde or 5-nitrosalicylaldehyde, respectively, with 1,2-bis(3-aminopropylamino) ethane and were crystallized with NO_3^- (1a/b), ClO_4^- (2a/b), PF_6^- (3a/b), CF_3SO_3^- (4a/b), and BPh_4^- (5a/b) counterions. Magnetostructural analysis reveals a minor trend in the spin state preference depending on the position of the nitro substituent where the orientation is dependent on crystal packing. Compounds using the 3- NO_2 -sal₂-323 ligand, H_2L_1 , where the nitro group is bent out-of-plane to the benzene ring of the Schiff base, tend to stabilize the triplet state, $S=1$, while those with the 5- NO_2 -sal₂-323 Schiff base, H_2L_2 , where the nitro group is almost perfectly aligned in-plane with the benzene ring, mostly stabilize the spin-quintet form, $S=2$. Density functional theory calculations correctly describe the energetics of intermediate spin/high spin transitions in the complexes. The intrinsic molecular magnetic properties are only marginally dependent on the position of the nitro groups; the out-of-plane orientation for the 3- NO_2 is stabilized by an intramolecular hydrogen bonding interaction between the nitro group and the equatorial sal ligand. This demonstrates that the control of magnetic behavior in the solid state is mainly a cooperative effect from the size and distribution of counterions, crystal packing, and intermolecular interactions. Three potential structural phase transitions were identified, in complexes 3a, 4a, and 5a · 2MeCN including one which is not coupled to a spin state change. Finally, a break in the pattern of Jahn-Teller distortion typical for $[\text{Mn}(\text{R-Sal}_2\text{-323})]^+$ complexes was observed in two of the complexes with the 5- NO_2 ligand, where elongation of the Mn–O bond lengths on warming replaced the usual pattern of elongation of only Mn–N distances.

© 2021 Author(s). All article content, except where otherwise noted, is licensed under a Creative Commons Attribution (CC BY) license (<http://creativecommons.org/licenses/by/4.0/>). <https://doi.org/10.1063/5.0050276>

I. INTRODUCTION

Facile access to more than one arrangement of d-electrons in spin crossover (SCO) transition metal complexes constitutes one of the most dramatic and highly developed examples of molecular bistability.^{1,2} SCO complexes are prized because of the ease by which they can be switched by many varied physical stimuli^{3–7} and because the profound differences in spectral and magnetic signatures between the two spin states make the switching easy to follow

on a range of timescales.^{8–10} The materials processing of SCO is the subject of intense investigation with many reports of surface attachment and primitive device preparation.^{2,11–13} Bousseksou *et al.* have recently shown that the challenge of sample fatiguability can be overcome by using high quality vacuum-deposition to prepare a thin film of an Fe^{2+} SCO complex, which is stable for more than one year and which can endure 10^7 switching cycles without loss of signal.¹⁴ This development has demonstrated that integration of

spin switchable complexes into current technologies such as nanothermometry is an achievable goal and will encourage further work toward this important outcome. However, despite the impressive advances in moving toward device preparation and real-world applications, less progress has been made in meeting the challenge of predicting or controlling SCO behavior. This is particularly true in the solid state where second coordination sphere effects and intermolecular interactions can facilitate or block access to more than one spin state. This has been demonstrated comprehensively in solid state $\text{Fe}^{2+/3+}$ systems where crystal engineering studies on thermal evolution SCO profiles abound.^{15–18} More progress on control and modulation has been achieved in soft media where Halcrow has reported a linear correlation between $T_{1/2}$ and Hammett parameters of the ligand substituents in $[\text{Fe}(\text{bpp})_2]^{2+}$ complexes (bpp is the N-heterocyclic ligand 2,6-di{pyrazol-1-yl}pyridine) in a range of solvents.^{19,20} A linear correlation between chain length and $T_{1/2}$ has also been observed in amphiphilic Fe^{2+} complexes in solution, with $T_{1/2}$ either increasing²¹ or decreasing²² with increasing alkyl chain length on the amphiphilic ligand. Less work has been reported in this area on Mn(III) where all studies to date have been in the solid state.²³ The primary ligand system that promotes thermal SCO in Mn(III) is the hexadentate Schiff base resulting from condensation of 1,2-bis(3-aminopropylamino)ethane with a substituted 2-hydroxybenzaldehyde and the ligand type is often abbreviated as R-Sal₂323 to indicate the 323 alkyl connectivity in the starting tetraamine and the substitution (R) on the phenolate ring. Our work on Mn(III) SCO with this ligand type^{24–35} includes a number of solid-state magnetostructural studies, which have demonstrated the importance of second coordination sphere effects in shaping the thermal evolution profile.^{24–28} However, a systematic analysis of the electronic effects of peripheral ligand substituents on Mn(III) SCO has so far been missing from our work and that with other ligand types.^{36–38} We address this now with a comprehensive magnetostructural comparative study of the effects of positioning strongly electron-withdrawing nitro groups *ortho* or *para* to the phenolate oxygen donor in the R-Sal₂323 coordination sphere. This results in a strong trend toward stabilization of the spin triplet form for the *ortho* nitro position in contrast to a tendency for stabilization of the spin quintet form when the nitro group is in the *para* position.

The prediction of the relative ordering of spin states in transition-metal complexes is still a challenge to current theoretical

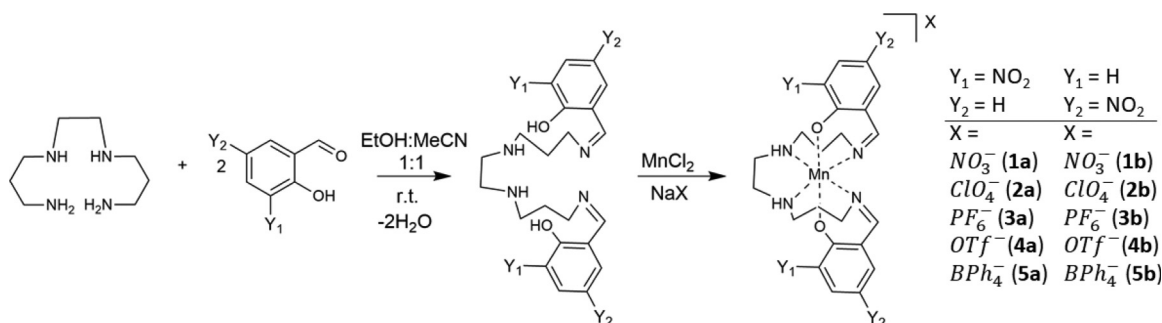
methods. Computational approaches to calculate structural and electronic effects upon switching the electronic state of molecules are commonly performed using Density Functional Theory (DFT) calculations,^{39–41} whereas large energetic splittings between different spin states can usually be well described with a number of DFT functionals, in particular, weak-field complexes with small energy differences between different spin multiplicities are a challenge.⁴² Recent benchmark calculations showed also that wavefunction based multireference methods or coupled cluster theory are not always superior to DFT calculations.^{43,44} Manganese(III) in the weak octahedral ligand field of a Schiff base complex has not received much attention from theoreticians. Rather, the quest for a possible $\Delta S = 2$ transition in a pentagonal bipyramidal coordination environment was investigated.⁴⁵

Here, we extend our previous work on intermediate to high-spin transitions in Mn(III) sal complexes²⁷ to include those with aromatic nitro substituents on the ligand. Intra- vs intermolecular interactions are mediated by small molecular distortions but largely determined by crystal packing effects to which counterions also contribute significantly.

II. RESULTS AND DISCUSSION

A. Synthetic approach

Two Schiff base ligands with nitro groups appended *ortho* (H_2L_1) or *para* (H_2L_2) to the phenolate oxygen donor were prepared by addition of 3- or 5-nitrosalicylaldehyde, respectively, in a 2:1 ratio with 1,2-bis(3-aminopropylamino)ethane (Scheme 1). A series of $[\text{MnL}]^+$ complexes with five counterions (1)–(5) was prepared with each ligand (3-nitro = “a” series; 5-nitro = “b” series), with occasional co-crystallization of solvent as detailed in the discussion of the structural and magnetic properties. The addition of a source of Mn(II) yielded dark red/black crystals of Mn(III) complexes (1a)–(5a) and (1b)–(5b) following aerial oxidation after standing for a few days. While nitrate and perchlorate complexes (1a/b) and (2a/b) were directly synthesized from the respective manganese(II) salt, complexes (3a/b)–(5a/b) with hexafluorophosphate, triflate, and tetraphenylborate were formed by a salt metathesis procedure with the target counterions introduced as their group 1 salts, for example, sodium as indicated in Scheme 1. This led to the successful crystallization of $[\text{MnL}_1]^+$, and $[\text{MnL}_2]^+$



SCHEME 1. Synthesis of $[\text{MnL}_1]\text{X}$ complexes (1a)–(5a) and $[\text{MnL}_2]\text{X}$ complexes (1b)–(5b).

respectively, in all the preferred crystal lattices. The structures of all compounds were established by single crystal x-ray diffraction, and the bulk samples were then fully characterized using elemental analysis, IR spectroscopy, and magnetic measurements. Due to the electron-withdrawing effect of the nitro substituents on the Schiff base ligand, it was also possible to stabilize the neutral Mn(II) complex in the 3-NO₂-sal₂-323 case, (6a), in low yields as a side product, the structure of which is reported here for completeness. For full synthetic details, see Sec. IV.

B. Magnetic characterization

The magnetic susceptibility of the bulk samples of compounds (1)–(5) in both the (a) and (b) series was measured using a SQUID magnetometer and the data were collected from 300.0 down to 5.0 K under an applied dc field of 5000 Oe, Fig. 1. No thermal hysteresis was detected on warming back to room temperature and plots of $\chi_M T$ vs T are shown in Figs. 1 and 2.

Magnetic data for nitrate complex (1a) are not available as there was insufficient bulk sample, but variable temperature diffraction data (see Sec. II C) indicate that nitrate complex (1a) has an $S = 1$ spin state at 100 K and only a small increase in the fraction of spin quintet form on warming to room temperature according to the bond length changes, i.e., a stabilization of the $S = 1$ state.

The magnetic data of Mn(III) complexes (2a)–(4a) with the *ortho*-substituted 3-NO₂-sal₂-323 Schiff base show a preference for the spin-triplet $S = 1$ state at low temperatures, Fig. 1, while both solvatomorphs with the tetraphenylborate counterion 5a · 2MeCN and 5a · 3MeCN show incomplete thermal SCO over the measured range. Compounds (2a)–(4a) are purely $S = 1$ below 100 K with a $\chi_M T$ value of 1.0 cm³K/mol, which fits to $S = 1$. Upon increasing

the temperature, there is an increase in the $\chi_M T$ product for all three although all are far from being fully high-spin by room temperature: the ClO₄[−] (2a) and PF₆[−] (3a) complexes reach a $\chi_M T$ value of about 2.0 cm³K/mol at room temperature, which indicates a 1:1 ratio between quintet:triplet spin state. The triflate salt (4a) only reaches a $\chi_M T$ value of 1.3 cm³K/mol at room temperature, indicating a 15% transition toward the high-spin state, but showing an upwards trend at 300 K. Both solvatomorphs of complex (5a) show a stepped transition in $\chi_M T$ at approximately 200 K (Fig. 1). Upon further cooling, the $\chi_M T$ product stabilizes at values of about 2.0 cm³K/mol, which usually is indicative of a 1:1 ratio of $S = 1$ and $S = 2$ states. The room temperature $\chi_M T$ value of both 5a · 2MeCN and 5a · 3MeCN does not reach the full high-spin value of 3.0 cm³K/mol. This shows that the magnetic behavior of complexes 1a to 5a in the crystal is not only determined by the molecular ligand field strength but also by the nature of the counterion and/or solvate molecules.

In marked contrast, the Mn(III) complexes with the *para*-substituted 5-NO₂-sal₂-323 Schiff base show a strong tendency to stabilize the spin-quintet state, $S = 2$, Fig. 2, with slightly different thermal responses within the set. Both solvated isostructural nitrate 1b · MeCN · 0.5H₂O and perchlorate 2b · MeCN · 0.5H₂O compounds show an incomplete transition between 150 and 293 K, with the low temperature $\chi_M T$ value of 2.0 cm³K/mol suggesting a 1:1 ratio of $S = 1$ and $S = 2$ components. A second solvatomorph of the perchlorate salt was isolated with half the amount of acetonitrile, 2b · 0.5MeCN · 0.5H₂O, and this sample persists in the spin-quintet state over the whole measured temperature range. While the triflate and tetraphenylborate salts (4b) and (5b) also remain in the HS state over the whole temperature regime, compound (3b), [MnL₂]PF₆, is the outlier of this family as it remains stubbornly

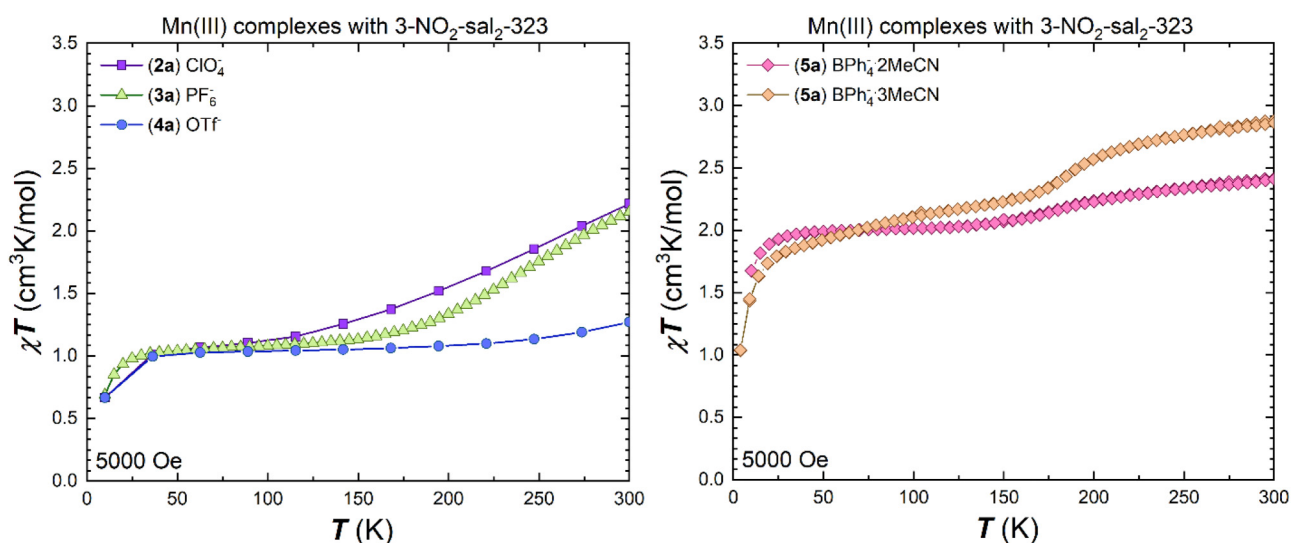


FIG. 1. Plots of $\chi_M T$ vs T for the complexes with the 3-NO₂-sal₂-323 ligand in the temperature range 5–300 K in cooling mode using an applied dc field of 5000 Oe: left: (2a) (purple), (3a) (green), (4a) (blue); right: data for the two different solvatomorphs of (5a) (orange, pink).

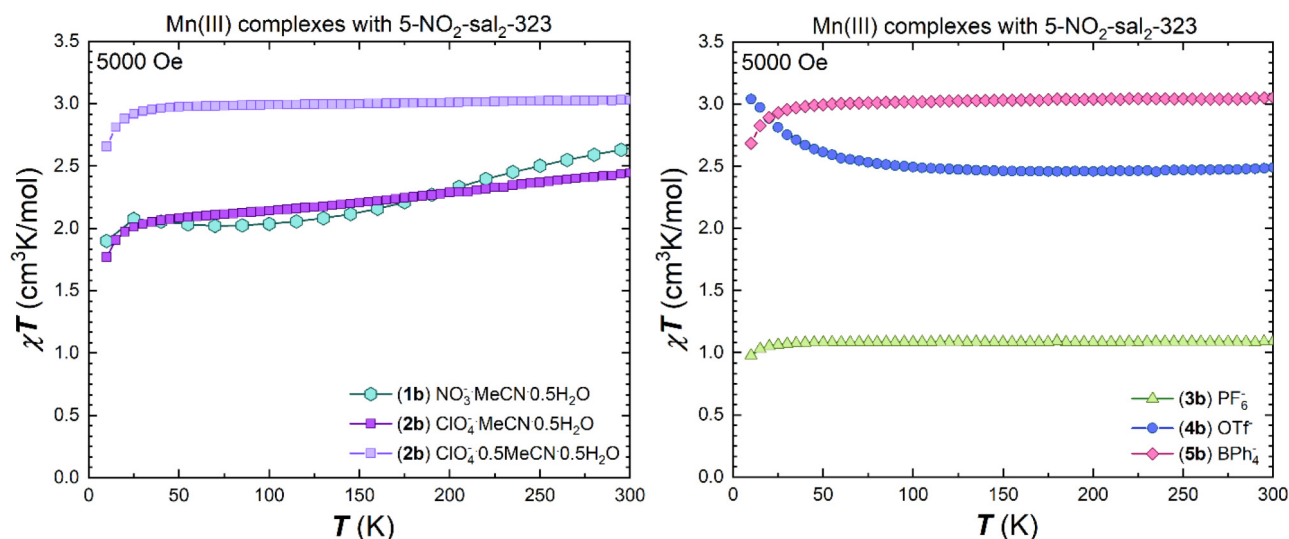


FIG. 2. Plots of $\chi_M T$ vs T for the complexes with the 5-NO₂-sal₂-323 ligand in the temperature range between 5 and 300 K in cooling mode using an applied dc field of 5000 Oe: left: (1b) (turquoise) and the two different solvatomorphs of (2b) (purple, violet); right: (3b) (green), (4b) (blue), and (5b) (pink).

and firmly in the spin-triplet state up to room temperature. The CF₃SO₃⁻ containing complex (4b) displays a gradual increase in $\chi_M T$ at very low temperatures, Fig. 2, which is tentatively attributed to onset of weak, long-range ferromagnetic ordering of the sample.

The apparent different magnetic properties of 3-NO₂ vs 5-NO₂-substituted complexes prompted the investigation of the difference in ligand field strengths of *ortho*- vs *para*-substitution (see Sec. II D).

C. Structural characterization

1. Crystal structures with *ortho*-substituted ligand 3-NO₂-sal₂-323: [MnL₁]⁺X, (1a)–(5a)

Compounds (1a)–(4a) crystallize solvent free while BPh₄⁻ complex (5a) crystallizes as either of two solvates with either two or three molecules of acetonitrile in the crystal lattice yielding 5a·2MeCN or 5a·3MeCN. Diffraction data on single crystals of all six compounds (1a)–(5a) (both solvatomorphs) were collected at 100 K and, in most cases, at a temperature higher than 100 K (Tables S1–S3). Due to a time lapse in data collections, a fresh crystal was used for the higher temperature data collections. In three cases of the PF₆⁻ (3a) CF₃SO₃⁻ (4a), and BPh₄⁻ 5a·2MeCN complexes, different unit cells were observed at the two temperatures (Tables S2 and S3 in the [supplementary material](#)). This may be due to a phase transition as the bond length differences between the two temperatures are in line with the observed magnetism and each is discussed in turn. It should be noted that only *two* of the three complexes in the 3-NO₂ series where there is a crystallographic difference between high and low temperature structures also show thermal SCO, that is, (3a) and (5a). The remaining complex, (4a), remains in a single spin state ($S = 1$) across the measured range, i.e., if the observed crystallographic change is due to a

phase transition, rather than the existence of polymorphs, then it is not accompanied by spin state switching. This would constitute the first such example of an uncoupled structural phase transition for Mn complexes of this type. However, as the crystals of all three complexes (3a), (4a), and (5a) were not cycled through a temperature gradient during the data collection, it cannot be stated definitively that the changes constitute phase transitions. This is the focus of current structural and spectroscopic investigations which are not reported here.

In all structures, the hexadentate Schiff base ligand chelates the Mn(III) ion with *pseudo*-octahedral geometry with two *trans*-phenolate donors, two *cis*-amine and two *cis*-imine donor atoms, in the same way as previously observed for manganese(III) complexes with this type of ligand.^{24–35} The structure of compound (1a) is shown in Fig. 3 as a representative example of the coordination sphere in compounds (1a)–(5a).

Complex (1a) crystallizes in the monoclinic space group Cc with $Z = 4$, where the asymmetric unit contains a full [MnL₁]⁺ cation and one full occupancy nitrate anion. The perchlorate complex (2a) crystallizes with $Z = 8$ in the monoclinic space group $P2_1/c$, with two full [MnL₁]⁺ cations and two well-ordered perchlorate anions as the asymmetric unit, and strong H-bonding between individual cations mediated *via* the perchlorate counter anion. At 174 K, the structure of complex (3a), [MnL₁]PF₆, was solved in monoclinic space group $C2/c$ with $Z = 4$. At 100 K, the structure was solved in related monoclinic space group $P2/c$ with $Z = 8$ and cell doubling along a suggesting a thermally induced structural phase transition. At both temperatures, the asymmetric unit comprises one octahedral Mn(III) complex cation and two half occupancy counterions both with an internal C_2 axis. Structural differences between the data collections of the triflate complex (4a) at high and low temperatures are more pronounced than for (3a)

with a change from space group $Pbca$ at 293 K to $Pna2_1$ at 100 K while $Z = 8$ remains the same. A full structural analysis of this compound across the thermal gradient will be completed as a separate study which is outside the scope of the current magnetostructural report. At room temperature, the asymmetric unit comprises one well-ordered full-occupancy $[\text{MnL}_1]^+$ cation charge balanced by one well-ordered full-occupancy triflate counterion in contrast to two full-occupancy $[\text{MnL}_1]^+$ cations and two full-occupancy triflate anions at 100 K, one with some disorder in the oxygen positions.

In a first round of synthesis, the BPh_4^- complex (5a) crystallized with two molecules of MeCN, 5a·2MeCN, and at 200 K the asymmetric unit comprises one well-ordered full-occupancy $[\text{MnL}_1]^+$ cation, one well-ordered full-occupancy tetraphenylborate counterion and two solvate molecules in monoclinic space group $P2_1/c$ with $Z = 8$. The asymmetric unit of the structure collected at 100 K on a new crystal indicates cell doubling along a with no change in space group but a new asymmetric unit comprising two well-ordered full-occupancy $[\text{MnL}_1]^+$ cations and tetraphenylborate counterions, Tables I and S3, along with the lattice solvent. A new solvatomorph with more acetonitrile, 5a·3MeCN, was recovered in an attempt to re-make the sample and data collections at 100 and 200 K with the new crystals did not show the cell-doubling of the crystals of di-solvated complex 5a·2MeCN. Instead, the asymmetric unit of 5a·3MeCN comprises one full occupancy $[\text{MnL}_1]^+$ cation and tetraphenylborate anion as well as three acetonitrile molecules in both data collections and this solvatomorph crystallizes in the monoclinic space group $P2_1/n$ with $Z = 4$. Finally, crystals of the Mn(II) complex with this ligand were also recovered, (6a), which crystallizes in the triclinic space group $P\bar{1}$ with $Z = 2$ with two molecules of water per Mn(II) complex. The asymmetric unit consists of one full occupancy Mn(II) complex and two full occupancy water molecules. Selected crystallographic data and structure refinements are summarized in Tables S1-S3 in the [supplementary material](#).

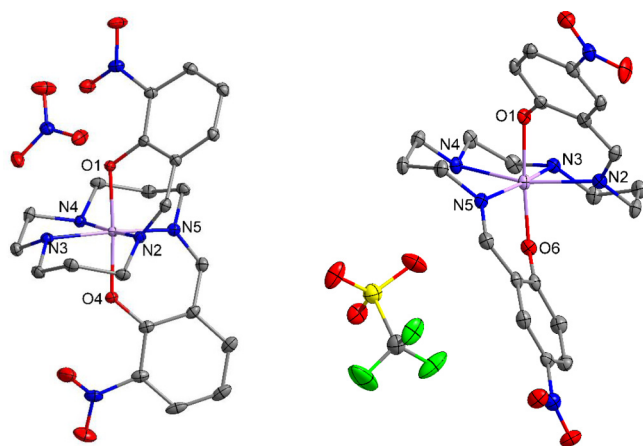


FIG. 3. Molecular structure of $[\text{MnL}_1]\text{NO}_3$ (1a) (left) and $[\text{MnL}_2]\text{CF}_3\text{SO}_3$ (4b) (right) measured at 100 K shown as an example for each series of compounds (hydrogen atoms omitted for clarity).

2. Crystal structures with para-substituted ligand 5-NO₂-sal₂-323: $[\text{MnL}_2]\text{X}$, (1b)–(5b)

In contrast to compounds (1a)–(5a), where only the BPh_4^- complex crystallized with solvation, two of the five salts of the complexes with para-substituted ligand 5-NO₂-sal₂-323, (1b)–(5b), crystallized with acetonitrile and water solvates, present to differing degrees. A single solvate of the nitrate complex, $[\text{MnL}_2]\text{NO}_3 \cdot \text{MeCN} \cdot 0.5\text{H}_2\text{O}$, (1b) was isolated and two solvates of the perchlorate complex, $[\text{MnL}_2]\text{ClO}_4 \cdot \text{MeCN} \cdot 0.5\text{H}_2\text{O}$ (2b·MeCN·0.5H₂O) and $[\text{MnL}_2]\text{ClO}_4 \cdot 0.5\text{MeCN} \cdot 0.5\text{H}_2\text{O}$ (2b·0.5MeCN·0.5H₂O), with different percentages of acetonitrile were recovered during the synthetic programme. The remaining compounds (3b)–(5b) crystallize solvent free and the structure of the cation of (4b) is shown in Fig. 3 as a representative example of the coordination sphere in compounds (1b)–(5b).

Compounds (1b), $[\text{MnL}_2]\text{NO}_3 \cdot \text{MeCN} \cdot 0.5\text{H}_2\text{O}$, and (2b), $[\text{MnL}_2]\text{ClO}_4 \cdot \text{MeCN} \cdot 0.5\text{H}_2\text{O}$, crystallize isostructurally in the triclinic space group $P\bar{1}$ with $Z = 2$ and data were collected at low and high temperature for both. At both measured temperatures, the asymmetric unit contains two unique cationic $[\text{MnL}_1]^+$ species as well as two respective anions. In addition, it was possible to crystallize (2b), $[\text{MnL}_2]\text{ClO}_4$, with less solvent, leading to 2b·0.5MeCN·0.5H₂O, which crystallizes in the tetragonal space group $P4/n$ with $Z = 4$. The asymmetric unit of complex 2b·0.5MeCN·0.5H₂O at 110 K comprises one discrete cation and one perchlorate counter anion which is modeled over three positions. It also contains one half of a highly distorted acetonitrile molecule, which is modeled over two sites while the half molecule of water is modeled over two locations, where one is overlapping with the oxygen of one ClO_4^- site.

The solvent-free complexes (3b)–(5b) all crystallize in different space groups and data were collected only at 100 K as magnetic data indicated that there was no spin state change for these three compounds. Complex (3b), $[\text{MnL}_2]\text{PF}_6$, crystallizes in the monoclinic space group $P2_1/n$ with $Z = 8$. There are two unique $[\text{MnL}_1]^+$ cations species as well as two anions within the asymmetric unit. At 100 K, one of the two hexafluorophosphate anions is well ordered while the other one shows significant disorder around the equatorial plane and the four equatorial fluorine atoms were modeled over 12 positions. Triflate complex (4b) crystallizes in monoclinic space group $P2_1/c$ with $Z = 4$, where the asymmetric unit contains one full $[\text{MnL}_1]^+$ cation and one triflate anion. The tetraphenylborate complex (5b) crystallizes in orthorhombic space group $Pna2_1$ with $Z = 4$ with one full $[\text{MnL}_1]^+$ cation and one full anion as the asymmetric unit. Selected crystallographic data and structure refinements of all compounds are summarized in Tables S4-S5 in the [supplementary material](#).

3. Thermal bond length changes in $[\text{MnL}_1]\text{X}$, (1a)–(5a)

The average bond lengths in Mn(III) SCO compounds of the $[\text{Mn}(\text{R-sal}_2\text{323})]^+$ type usually show a significant increase upon spin transition, but only significantly for the amine and imine bonds in the equatorial positions.^{23–35} The Mn–N_{imine} bond lengths are typically 1.95–2.00 Å in the $S = 1$ state, increasing to 2.05–2.18 Å within the $S = 2$ state, while the Mn–N_{amine} bond lengths change from 2.03–2.10 Å to 2.18–2.30 Å upon spin

TABLE I. Mn-donor bond lengths in complexes (1a)–(5a).

Mn-X	NO ₃ ⁻ (1a)	ClO ₄ ⁻ (2a)	PF ₆ ⁻ (3a)	OTf ⁻ (4a)	BPh ₄ ⁻ ·2MeCN (5a)	BPh ₄ ⁻ ·3 MeCN (5a)
Temp (K)	293	>100 ^a	174	293	200	200
Mn-O _{phen}	1.908	...	1.868	1.929	1.874	1.878
	1.911	...	1.873	1.932	1.875	1.888
Mn-N _{imine}	1.994	...	2.005	2.011	2.038	2.060
	2.003	...	2.014	2.055	2.088	2.098
Mn-N _{amine}	2.045	...	2.083	2.079	2.135	2.163
	2.053	...	2.090	2.122	2.185	2.180
spin state	S = 1	...	S = av	S = av	S = av	S = av
100 K		Mn1 Mn2		Mn1 Mn2	Mn1 Mn2	
Mn-O _{phen}	1.895	1.872; 1.887	1.870	1.888; 1.883	1.880; 1.866	1.880
	1.891	1.874; 1.896	1.881	1.893; 1.887	1.890; 1.877	1.890
Mn-N _{imine}	1.987	1.982; 1.987	1.986	1.985; 1.991	1.989; 2.072	2.026
	1.986	1.989; 1.995	1.991	1.989; 1.995	1.998; 2.146	2.060
Mn-N _{amine}	2.040	2.055; 2.057	2.053	2.044; 2.051	2.056; 2.174	2.121
	2.040	2.057; 2.060	2.056	2.051; 2.053	2.062; 2.268	2.130
spin state	S = 1	S ₁ = 1; S ₂ = 1	S = 1	S ₁ = 1; S ₂ = 1	S ₁ = 1; S ₂ = 2	S = av

^aNot measured.

transition. The bond lengths of (1a)–(5a) are summarized in Table I to show thermal bond length changes. Complexes (1a), (3a), and solvatomorph 5a.3MeCN all have one Mn site at high and low temperatures and the bond length changes broadly support the observed magnetism, i.e., stabilization of mainly the S = 1 assignment for (1a) and (3a) and small variation of the spin

state ratio within an average S = 1 and S = 2 state in the BPh₄⁻ complex 5a.3MeCN across the measured range. A room temperature structure of [MnL₁]ClO₄ (2a) could not be obtained but at 100 K this complex has two unique Mn(III) sites with bond lengths in both indicative of spin triplet d⁴ in line with the SQUID data. As discussed above, there is a change in symmetry between the high

TABLE II. Mn-donor bond lengths in complexes (1b)–(5b).

Mn-X	NO ₃ ⁻ ·MeCN· 0.5 H ₂ O (1b)	ClO ₄ ⁻ ·MeCN· 0.5 H ₂ O (2b)	ClO ₄ ⁻ ·0.5 MeCN· 0.5 H ₂ O (2b)	PF ₆ ⁻ (3b)	OTf ⁻ (4b)	BPh ₄ ⁻ · 2 MeCN (5b)
	293	260	>100 ^a	>100 ^a	>100 ^a	>100 ^a
Temp (K)	Mn1 Mn2	Mn1 Mn2		Mn1 Mn2		
Mn-O _{phen}	1.942; 1.875	1.908; 1.875
	1.957; 1.871	1.919; 1.884
Mn-N _{imine}	2.096; 2.117	2.014; 2.081
	2.018; 2.105	2.019; 2.151
Mn-N _{amine}	2.070; 2.234	2.064; 2.217
	2.121; 2.210	2.073; 2.269
spin state	S ₁ = av; S ₂ = 2	S ₁ = av; S ₂ = 2				
100 K						
Mn-O _{phen}	1.898; 1.872	1.893; 1.870	1.873	1.882; 1.882	1.864	1.872
	1.898; 1.878	1.899; 1.876	1.875	1.891; 1.883	1.887	1.877
Mn-N _{imine}	1.999; 2.080	1.987; 2.063	2.103	1.984; 1.990	2.049	2.083
	2.000; 2.133	1.996; 2.153	2.127	1.993; 2.007	2.168	2.141
Mn-N _{amine}	2.043; 2.177	2.037; 2.195	2.237	2.033; 2.041	2.170	2.205
	2.047; 2.241	2.046; 2.269	2.272	2.046; 2.061	2.241	2.278
Spin state	S ₁ = 1; S ₂ = 2	S ₁ = 1; S ₂ = 2	S = 2	S ₁ = 1; S ₂ = 1	S = av	S = 2

^aNot measured.

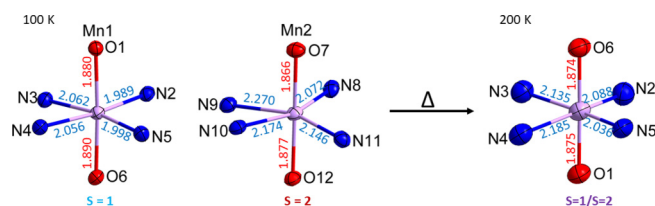


FIG. 4. Observed bond length changes within $5a \cdot 2\text{MeCN}$ by increasing the temperature from 100 K [two Mn(III) sites] to 200 K [one single Mn(III) site].

and low data collections in the CF_3SO_3^- (**4a**) and BPh_4^- $5a \cdot 2\text{MeCN}$ SCO complexes. In the higher temperature data collections, both have a single Mn site with bond lengths suggestive of an averaged spin state site in each, in line with the magnetic data at the same temperatures.

The data collections of (**4a**) and $5a \cdot 2\text{MeCN}$ at 100 K are cell doubled with respect to the higher temperature data sets and the two unique sites in triflate complex (**4a**) correspond well to $S=1$ SQUID assignment. In contrast, the two unique sites in the $5a \cdot 2\text{MeCN}$ complex are clearly in different spin states, the $S=1$ and $S=2$ sites clearly visible from the short and long bond distances in Mn1 and Mn2, respectively. An unusual feature in the 100 K structure of $5a \cdot 2\text{MeCN}$ is that the HS sites (Mn2) have significantly longer bond lengths than those in the averaged triplet/quintet form at 200 K, Fig. 4, a feature that has not been observed in iron SCO complexes with similar cell doubling.

As expected for the divalent Mn complex, (**6a**) Mn-donor bond lengths are longer in comparison to the Mn(III) compounds. The 3- NO_2 -sal₂-323 Mn(II) complex (**6a**) exhibits Mn- O_{phen} bond lengths between 2.12 and 2.14 Å, Mn- N_{imine} bond lengths between 2.23 and 2.24 Å, and Mn- N_{amine} bond lengths between 2.28 and 2.30 Å.

4. Thermal bond length changes in $[\text{MnL}_2]\text{X}$, (**1b**)-(5b)

On the other hand, the predominantly HS complexes obtained with the 5- NO_2 -sal₂-323 Schiff base generally exhibit longer bond lengths, Table II. The exception is the PF_6^- complex, (**3b**), which

has bond lengths typical for $S=1$ in both unique Mn sites at 100 K, matching the data obtained by magnetometry.

This is in sharp contrast to the BPh_4^- and CF_3SO_3^- analogs (**4b**) and (**5b**), which are close to or fully HS according to SQUID data and which have bond lengths with a good match,^{24–35} Table II. The perchlorate solvatomorph $2b \cdot 0.5\text{MeCN} \cdot 0.5\text{H}_2\text{O}$ is also fully HS according to the magnetism and this is borne out well in the bond lengths at 100 K. The last two complexes in this series are the isostructural nitrate and perchlorate solvatomorphs $1b \cdot \text{MeCN} \cdot 0.5\text{H}_2\text{O}$ and $2b \cdot \text{MeCN} \cdot 0.5\text{H}_2\text{O}$. Both show a gradual and incomplete thermal SCO over the measured range, Fig. 2, and the bond length changes observed here are different from the pattern established in the previously published examples of SCO in the wider set of $[\text{Mn}(\text{R-Sal}_2\text{-323})]^+$ complexes, which usually exhibit Mn-O bond lengths between 1.85 and 1.90 Å.²³ The structures of $1b \cdot \text{MeCN} \cdot 0.5\text{H}_2\text{O}$ and $2b \cdot \text{MeCN} \cdot 0.5\text{H}_2\text{O}$ both contain two unique Mn sites at high and low temperature with one site clearly $S=1$ and the other $S=2$ at 100 K, Table II. On warming, there are only minor increases in the $S=2$ site whereas those in the other sites change more markedly with significant increases in Mn-O distances observed for the first time. In the case of the nitrate complex, this is accompanied by an increase in bond lengths along the $\text{N}(4)_{\text{amine}}\text{-Mn}(1)\text{-N}(2)_{\text{amine}}$ axis indicating possible axial compression along the other $\text{N}(3)_{\text{amine}}\text{-Mn}(1)\text{-N}(5)_{\text{imine}}$ axis (Table II and Fig. 5). This suggests that the distortion in the HS form of the Mn1 complex cation is a Jahn-Teller compression with the $d_{x^2-y^2}$ orbital projected in the N_2O_2 plane, an arrangement that has not previously been observed with this ligand type.

5. Distortion parameters within $[\text{MnL}_1]\text{X}$, (**1a**)-(5a) and $[\text{MnL}_2]\text{X}$, (**1b**)-(5b)

Mononuclear hexacoordinated Mn(III) compounds exhibit a stronger distortion of the octahedral environment in the spin quintet state than in the almost perfect octahedral shape observed in the triplet spin state due to the Jahn-Teller effect. The degree of distortion can be analyzed by the distortion parameters Σ and Θ as defined by McKee *et al.*⁴⁶ Σ highlights the local angular deviation from the *cis* octahedral angles of 90° , while Θ measures the trigonal torsion, which is defined as the degree of twist from a perfect octahedron towards trigonal prismatic geometry. Both values are zero in the case of a perfect octahedron. The values for Σ and Θ for

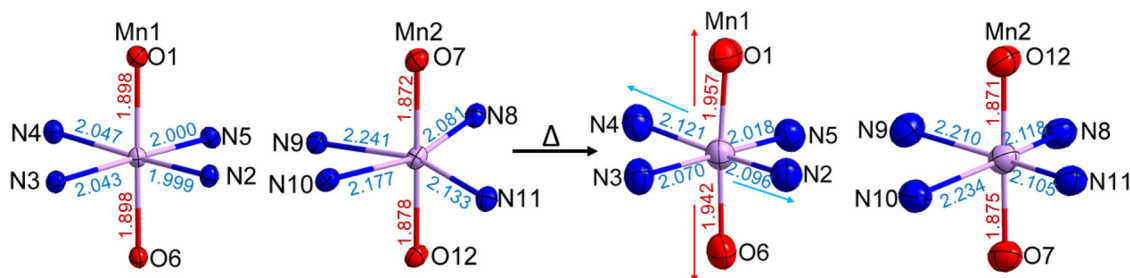


FIG. 5. Metal coordination sphere of the two Mn(III) sites of $1b \cdot \text{MeCN} \cdot 0.5\text{H}_2\text{O}$ at 100 K (left) and 293 K (right), highlighting the bond length changes (in Å) upon heating.

TABLE III. Distortion angle parameters, Σ (angular deviation at the origin) and Θ (trigonal torsion angle) for all $[\text{MnL}_1]\text{X}$ complexes (1a)–(5a).

	NO_3^- (1a)	ClO_4^- (2a)	PF_6^- (3a)	OTf^- (4a)	$\text{BPh}_4^- \cdot 2 \text{ MeCN}$ (5a)	$\text{BPh}_4^- \cdot 3 \text{ MeCN}$ (5a)
Temp. (K)	100	100	100	100	100	100
	Mn	Mn1 Mn2	Mn	Mn1 Mn2	Mn1 Mn2	Mn
Σ	31.3	31.6; 31.6	35.1	28.2; 37.3	32.7; 99.4	50.2
Θ	89.9	90.6; 97.0	102.1	83.9; 104.2	75.5; 259.8	161.8
Spin state	$S = 1$	$S_1 = 1; S_2 = 1$	$S = 1$	$S_1 = 1; S_2 = 1$	$S_1 = 1; S_2 = 2$	$S = 2$
Temp. (K)	293		174	293	200	200
Σ	33.5		44.4	45.7	57.7	60.0
Θ	97.8		131.2	164.4	191.3	201.5
Spin state	$S = 1$		$S = \text{av}$	$S = \text{av}$	$S = \text{av}$	$S = \text{av}$

mononuclear Mn(III) compounds are in the range of $\Sigma = 28^\circ\text{--}45^\circ$ for $S = 1$ ($\Sigma = 48^\circ\text{--}70^\circ$ for $S = 2$) and $\Theta = 79^\circ\text{--}125^\circ$ for $S = 1$ ($\Theta = 135^\circ\text{--}230^\circ$ for $S = 2$).^{25,27} Both Σ and Θ have been calculated for all compounds using OctaDist,⁴⁷ and the values are summarized in Tables III and IV. These distortion parameters are in line with the observed magnetic properties.

Compounds (1a)–(4a) with the 3- NO_2 -sal₂-323 Schiff base, $[\text{MnL}_1]^+$, exhibit values that are indicative of an $S = 1$ spin state at 100 K with Σ values in the range between 28.2° and 37.3° at 100 K, and the Θ values between 83.9° and 104.2° , where the highest and lowest of both sets of values were found within $[\text{MnL}_1]\text{OTf}$ (4a) (see Table III). Upon increasing the temperature, all four compounds (1a)–(4a) show higher distortion values, which is in line with the increase in the magnetic moment with increasing temperature. The coordination sphere of (1a) is shown in Fig. 6 as an example of the spin triplet compounds (1a)–(4a), to highlight the small distortion from the perfect octahedral environment. In the case of the two solvatomorphs of compound (5a), 5a-2MeCN and 5a-3MeCN, both sets of Σ and Θ values indicate that there is less distortion at 100 K than at 200 K. At 100 K, the Σ and Θ values of 5a-3MeCN are at the lower end of the value range that are indicative of a HS Mn(III) center. The difference in value between the two temperatures is large enough to indicate a gradual transition, which matches the observed magnetic properties. Interestingly, while the distortion parameters of 5a-2MeCN clearly show one pure $S = 2$ and one pure $S = 1$ site, where the values of the HS site are on the higher end of the

spectra, the 200 K structure only contained one Mn(III) site, which is HS but shows less distortion than HS site of 100 K. While these Σ and Θ values help to estimate the spin state, they are not very accurate to determine if a complex has reached the full saturated high-spin state yet. Even though the Σ and Θ values of 5a-2MeCN and 5a-3MeCN indicate that at 200 K both compounds resemble an $S = 2$ Mn(III) complex in its disordered way, it does not entirely reflect the magnetic profile, which is not saturated at this temperature. 5a-2MeCN has reached 62% of the expected HS value ($2.235 \text{ cm}^3 \text{ K/mol}$ at 200 K), while 5a-3MeCN is already 80% in the HS state ($2.568 \text{ cm}^3 \text{ K/mol}$ at 200 K), which is dominantly HS, but not fully yet, but cannot be determined by a numerical value of distortion parameters.

Compounds (1b)–(5b) using the 5- NO_2 -sal₂-323 Schiff base, $[\text{MnL}_2]^+$, exhibit Σ and Θ values that are mostly indicative of an $S = 2$ spin state, with the exception of compound (3b), that is solely $S = 1$, see Table IV. The high-spin Mn(III) sites at 100 K show Σ values in the range between 65.8° and 95.2° at 100 K, and Θ values between 270.0° and 328.9° . The two structures that are measured at increased temperatures, 1b-1MeCN-0.5H₂O and 2b-1MeCN-0.5H₂O, show an increase of Σ values up to 80.65° for (1b) and 113.07° for (2b), while the increase in Θ values is less pronounced. Compounds (1b) and (2b), 1b-1MeCN-0.5H₂O and 2b-1MeCN-0.5H₂O, each contain one spin triplet and one spin quintet cation which is reflected in the distortion parameters. Upon increasing the temperature, there is an increase in distortion clearly visible within the former $S = 1$ site, see Table IV.

TABLE IV. Distortion angle parameters, Σ (angular deviation at the origin) and Θ (trigonal torsion angle) for all $[\text{MnL}_2]\text{X}$ complexes (1b)–(5b).

	$\text{NO}_3^- \cdot \text{MeCN} \cdot 0.5 \text{ H}_2\text{O}$ (1b)	$\text{ClO}_4^- \cdot \text{MeCN} \cdot 0.5 \text{ H}_2\text{O}$ (2b)	$\text{ClO}_4^- \cdot 0.5 \text{ MeCN} \cdot 0.5 \text{ H}_2\text{O}$ (2b)	PF_6^- (3b)	OTf^- (4b)	BPh_4^- (5b)
Temp. (K)	100	100	100	100	100	100
Σ	30.9; 78.4	29.6; 95.2	87.3	31.3; 35.9	65.8	77.7
Θ	103.6; 270.0	87.2; 304.8	329.0	90.3; 110.1	251.3	280.4
Spin state	$S_1 = 1; S_2 = 2$	$S_1 = 1; S_2 = 2$	$S = 2$	$S_1 = 1; S_2 = 1$	$S = 2$	$S = 2$
Temp. (K)	293	260				
Σ	44.5; 80.7	35.96; 113.1				
Θ	159.5; 284.6	87.80; 312.5				
Spin state	$S_1 = \text{av}; S_2 = 2$	$S_1 = 1; S_2 = 2$				

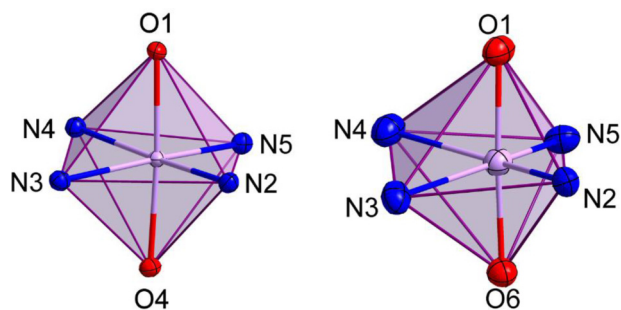


FIG. 6. Coordination polyhedron around the central Mn(III) center of $[\text{MnL}_1]\text{NO}_3$, (**1a**) (left) and the solvatomorph of $[\text{MnL}_2]\text{ClO}_4$, (**2b**), $2\text{b} \cdot 0.5\text{MeCN} \cdot 0.5\text{H}_2\text{O}$ (right) (both measured at 100 K) showing the small distortion of the almost perfect octahedral environment within the $S = 1$ form of (**1a**) and the high distortion of the high-spin $2\text{b} \cdot 0.5\text{MeCN} \cdot 0.5\text{H}_2\text{O}$.

Olguin has recently summarized the Σ values of complexes of the $[\text{Mn}(\text{R-Sal}_2\text{-323})^+]$ type, which highlight that compounds where the Mn(III) ion exhibits Σ values above 70° are often, but not always, locked in the high-spin state.²³ On the other hand, the Θ values might be a better indicator to detect molecules that cannot undergo a spin transition and are locked in the $S = 2$ state. We recently have discussed the possibility that compounds with Θ values greater than 250° are considered to be restrained to the $S = 2$ spin state and are not able to undergo spin transition.²⁸ This hypothesis is supported by the Θ values of the compounds using 5- NO_2 -sal₂-323, $[\text{MnL}_2]^+$ (see Table IV) especially the $[\text{MnL}_2]\text{ClO}_4$ solvatomorph $2\text{b} \cdot 0.5\text{MeCN} \cdot 0.5\text{H}_2\text{O}$, $[\text{MnL}_2]\text{OTf}$ (**4b**) and $[\text{MnL}_2]\text{BPh}_4$ (**5b**), which are constrained to the high spin state over the whole measured temperature range, and exhibit Θ values between 251.3° and 328.9° . The higher distortion values within $2\text{b} \cdot 0.5\text{MeCN} \cdot 0.5\text{H}_2\text{O}$ in comparison to the almost perfect octahedral environment of (**1a**) are depicted in Fig. 6. Similarly, the high-spin Mn(III) sites within compounds $1\text{b} \cdot 1\text{MeCN} \cdot 0.5\text{H}_2\text{O}$ and $2\text{b} \cdot 1\text{MeCN} \cdot 0.5\text{H}_2\text{O}$ exhibit quite large Θ values (270.0° – 312.5°), which keeps this Mn2 site locked in the HS state, while only the Mn1 site can undergo spin transition.

6. Twist of the NO_2 groups within $[\text{MnL}_1]\text{X}$, (**1a**)–(**5a**) and $[\text{MnL}_2]\text{X}$, (**1b**)–(**5b**)

The novel feature of the results presented here is the emergence of a trend relating electronic character of the ligand and choice of spin state in the coordinated d^4 ion, the first clear indication of a strong electronic effect in guiding manganese spin state choice. Both ligands L_1 and L_2 contain a nitro group capable of conjugation with the aromatic ring. The introduction of nitro group substituents influences the electronic structure of the benzene rings due to the strongly electron-attracting (EA) character. The EA ability is a result of both strong inductive and resonance activities (see also Sec. II D).

We have therefore considered the degree of conjugation in the two complex series as measured by the degree of torsional

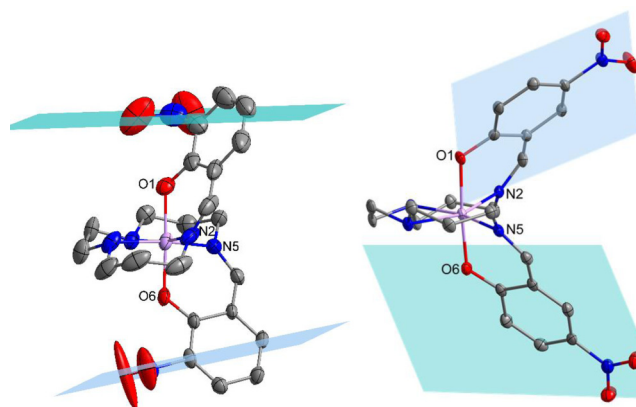


FIG. 7. Twist of the NO_2 groups out-of-plane of the benzene ring of the Schiff base ligand of the cationic Mn(III) species of (**3a**), $[\text{MnL}_1]\text{PF}_6$, (at 174 K) (left) and the in-plane arrangement in HS (**4b**), $[\text{MnL}_1]\text{OTf}$ at 100 K (right).

distortion of the nitro groups relative to the phenol rings and compared this to the choice of spin state. This analysis reveals that while the nitro group of the Schiff base ligand is flipped out-of-plane for most of the complexes with the *ortho* substitution of the NO_2 -group, those with the *para*-substituted ligands have the nitro group mostly in-plane with the benzene ring of the respective Schiff base, see Fig. 7. The twist is measured as the angle between the plane of the benzene ring and the plane of the NO_2 group leading to a maximum twist of 90° when the nitro group is perpendicular to the benzene ring. The twist angles for both sets of compounds are summarized in Tables V and VI.

The angles between the plane of the NO_2 group in the 3-position and the benzene ring of the Schiff base ligand within complexes (**1a**) to (**5a**) are in the range between 20° and 73° (see Table V), highlighting the out-of-plane character of the nitro substituents within this family of compounds. This may be accompanied by formation of intramolecular H-bonds. Each nitro substituent shows a distinct set of close contacts between the oxygen atoms of the nitro group and nearby hydrogen atoms. Depending on the angle of twist of the nitro group, the intramolecular interactions range between one and two close contacts per nitro group. In order to establish intramolecular H-bonds, within the range of 2.2 – 2.5 Å, the nitro group can be rotated out-of-plane of the benzene ring, which can lead to the establishment of a close contact with a hydrogen on the neighboring carbon of the benzene ring, as observed within (**1a**) and (**4a**) (see Fig. S1 in the supplementary material). The flexibility of the nitro substituent is observed within the disorder of the oxygen atoms of the nitro group in (**4a**) and (**5a**), highlighting the high degree of freedom of the substituent's position. The twist angle of the nitro group may enable several close contacts allowing the creation of up to two H-bonds to both oxygen atoms of the nitro substituent. Figure S1 in the supplementary material shows the potential intramolecular H-bonds, which are observed within $[\text{MnL}_1]\text{NO}_3$ at both measured temperatures, 100 K and 293 K, respectively. Both structures display intramolecular close contacts

TABLE V. Angle between the plane of the NO₂ group in the 3-position and the benzene ring of the Schiff base ligand for all [MnL₁]X complexes (1a)–(5a).

	NO ₃ ⁻ (1a)	ClO ₄ ⁻ (2a)	PF ₆ ⁻ (3a)	OTf ⁻ (4a)	BPh ₄ ⁻ · 2 MeCN (5a)	BPh ₄ ⁻ · 3 MeCN (5a)
Temp. (K)	100	100	100	100	100	100
	Mn	Mn1 Mn2	Mn	Mn1 Mn2	Mn1 Mn2	Mn
Sal1-NO ₂	22.60°	38.27°; 56.30°	41.89°	56.50°; 50.21°	57.14°; 82.61°	46.06°
Sal2-NO ₂	33.66°	40.19°; 67.59°	60.08°	16.05°; 52.5° ^a	41.62°; 63.93°	60.79°
Temp. (K)	293		174	293	200	200
Sal1-NO ₂	20.07°		63.24°	27.62°	53.93°	48.41°
Sal2-NO ₂	37.18° ^b		73.66°	1.76°	65.55° ^c	62.72°

^a(4a) exhibits a disorder of the NO₂ group of the salicylaldehyde of O12 within the Mn2 site (100 K). The two positions are crystallographically weighted 0.33:0.66 leading to angles of 59.93°:49.56°, weighted average is used.

^b(1a) exhibits a disorder of the NO₂ group of the salicylaldehyde of O4 (293 K). The two positions are crystallographically weighted 0.79:0.21 leading to angles of 37.40°:36.35°; therefore, the weighted average is used.

^c(5a) exhibits a disorder of both oxygen atoms of the NO₂ group, O5 and O6 (200 K). The two positions are crystallographically weighted 0.44:0.55 leading to angles of 64.57°:67.52°; therefore, the weighted average is used.

to one direct neighboring CH of the benzene ring, as well as to one of the CH₂ groups of the propylene backbone of the Schiff base ligand.

[MnL₁]ClO₄, (2a), shows that within site 1, around Mn1, only one of the two nitro groups, that with a twist angle of 40.2°, forms a short contact with a propylene hydrogen, see Fig. S2 in the [supplementary material](#). In contrast both nitro groups in the Mn2 complex cation form short contacts, Fig. S2 in the [supplementary material](#), and these also have higher twist angles of 56.3° and 67.6°.

Interestingly, no such possible intramolecular H-bonds in the range of 2.2–2.5 Å can be observed within complex (3a), [MnL₁]PF₆, where the nitro groups also exhibit large twist angles at both temperatures (see [Table V](#)). This shows that the possibility of establishing intramolecular H-bonds is not only dependent on the twisting angle of the nitro substituent, but also dependent on the angle of the benzene ring in relation to the tetraamine backbone. While the tetraamine backbone arranges in a similar fashion within this family of compounds, the benzene rings of the Schiff base ligands can tilt in order to accommodate the

crystal packing, which in the case of (3a) blocks formation of short contacts with the nitro substituents and adjacent hydrogens (see Fig. S3 in the [supplementary material](#)). At increased temperature (174 K), the out-of-plane twist angles of the nitro substituents within (3a) increase to 63.2° and 73.7°. While the major part of the [MnL₁]⁺ cation remains unchanged, only the twist angle increases (see Fig. S4 in the [supplementary material](#)), highlighting the flexibility of the nitro group to rotate, once there are no H-bonds involved.

The smallest twist angle in the three-nitro series can be found within the room temperature structure of [MnL₁]OTf (4a), where one of the two nitro groups, around N6, is almost perfectly aligned in-plane with the benzene ring of the Schiff base (a twist angle of 1.76°) showing similar intramolecular H-bonds as observed within [MnL₁]NO₃, (1a) (see Fig. S5 in the [supplementary material](#)). The second nitro group around N1 exhibits a higher distortion of 27.6°, which is possibly due to the two competing interactions to two of the hydrogen atoms of C13 and C15 within the propylene group of the Schiff base backbone (see Fig. S5 in the [supplementary material](#)). By decreasing the temperature to 100 K, [MnL₁]OTf (4a)

TABLE VI. Angle between the plane of the NO₂ group in the 5-position and the benzene ring of the Schiff base ligand for all [MnL₂]X complexes (1b)–(5b).

	NO ₃ ⁻ · MeCN · 0.5 H ₂ O (1b)	ClO ₄ ⁻ · MeCN · 0.5 H ₂ O (2b)	ClO ₄ ⁻ · 0.5 MeCN · 0.5 H ₂ O (2b)	PF ₆ ⁻ (3b)	OTf ⁻ (4b)	BPh ₄ ⁻ (5b)
Temp. (K)	100	100	100	100	100	100
	Mn1 Mn2	Mn1 Mn2	Mn	Mn1 Mn2	Mn	Mn
Sal1-NO ₂	3.04°; 4.11°	2.22°; 3.38°	8.01°	19.39°; 19.69°	4.26°	18.56°
Sal2-NO ₂	5.59°; 3.10°	5.98°; 7.68°	2.16°	4.36°; 7.43°	5.01°	17.81°
Temp. (K)	293	260				
	Mn1 Mn2	Mn1 Mn2				
Sal1-NO ₂	1.62°; 3.74°	1.93°; 3.47°				
Sal2-NO ₂	5.21°; 6.26°	5.34°; 12.17°				

where there are two unique cationic Mn(III) cations in the crystal lattice, both sites exhibit higher twist angles of the nitro substituents, see Table V. These two sites show a similar trend as has been observed for $[\text{MnL}_1]\text{ClO}_4$ (**2a**). One Mn(III) site, around Mn2, only exhibits one intramolecular H-bond to a carbon of the tetraamine backbone, while the second site, around Mn1, shows intramolecular H-bonds to both nitro groups, as well as both phenol oxygen atoms (see Fig. S6 in the supplementary material).

The two solvatomorphs of $[\text{MnL}_1]\text{BPh}_4$ (**5a**) also show short contacts which could be indicative of intramolecular H-bond formation. At 100 K, the **5a-2MeCN** structure contains two sites, in which each site displays short contacts only for one nitro substituent of the Schiff base ligand, as well as additional intramolecular H-bonds between one phenol oxygen per cationic site to the tetraamine backbone (see Fig. S7 in the supplementary material). In the higher temperature structure, **5a-2MeCN** only has one unique cation in the unit cell, and the intramolecular H-bonds are reduced to one oxygen of one nitro group. This nitro group, around N6, exhibits a disorder of both oxygen atoms over two positions, where only the 0.44% occupancy component of the disorder can establish short contacts to the tetraamine backbone of the Schiff base ligand (see Fig. S8 in the supplementary material). On the other hand, the second solvatomorph of $[\text{MnL}_1]\text{BPh}_4$ (**5a**) containing three molecules of acetonitrile, **5a-3MeCN** exhibits only one single intramolecular interaction at both measured temperatures between one oxygen of the nitro substituent (twist angles of 60.8° at 100 K and 62.7° at 200 K) and the tetraamine backbone of the Schiff base ligand (see Fig. S9 in the supplementary material).

The angles between the plane of the NO_2 group in the 5-position and the benzene ring of the Schiff base ligand within complexes (**1b**) to (**5b**) are in most cases smaller than 10° , highlighting the in-plane character of the nitro substituents within this family of compounds. Moving the nitro substituent to the 5-position of the salicylaldehyde prevents the formation of intramolecular interactions with the tetraamine backbone of the Schiff base, while only short contacts to the direct neighboring carbons of the benzene ring can be formed, usually with both oxygen atoms of the nitro substituent (see Fig. S10 in the supplementary material).

$[\text{MnL}_2]\text{BPh}_4$ (**5b**) shows exceptionally large twist angles for this family of compounds with values of 17.8° and 18.6° , for the two nitro groups (see Table VI). Interestingly, the biggest out-of-plane deviation within this family of compounds was observed within $[\text{MnL}_2]\text{PF}_6$ (**3b**), where both Mn(III) sites exhibit one nitro group almost perfectly aligned in-plane (4.36° and 7.43°) while the second one is tilted out-of-plane with angles of 19.39° and 19.69° , which may be a contributory factor to the exceptional spin state choice of $S = 1$ within the five-nitro complex series where the other members were all high spin.

D. Computational section

Computationally, we are addressing here the intrinsic magnetic molecular properties of the 3- and 5-nitrosalicylaldehyde and 1,2-bis(3-aminopropylamino)ethane condensates. In the absence of packing effects in the crystalline states and the influence of counterions, the effect of the position of the nitro groups at 3- and 5-positions on the triplet-quintet splitting can be investigated.

Aromatic nitro groups are strongly electron-withdrawing ligands with both strong inductive (-I) and resonance (-M) activities due to their high electronegativity. The nitro group acts as π -acceptor by removing electron density from the adjacent aromatic π -electron system. We thus investigate the influence of the nitro-group positional and orientational dependence on the spin state splitting. Here, triplet and quintet states are termed intermediate spin (IS) and high spin (HS) in the computational analysis.

1. Influence of substituent positioning

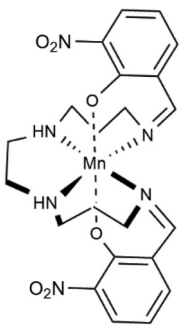
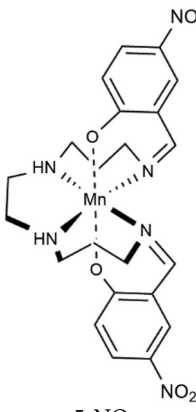
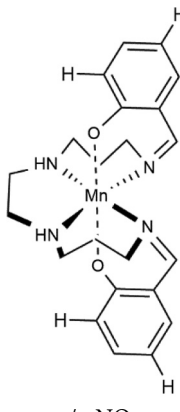
The calculated IS/HS changes in Gibbs free energies are summarized in Table VII. ΔG_{therm} are the thermodynamic corrections to the electronic energy differences ΔE to then give the change in Gibbs free energy upon SCO ($\Delta G_{\text{SCO(HS-IS)}}$). ΔG_{therm} is negative due to the increase in vibrational entropy and zero-point vibrational energy upon elongation of the amine and imine Mn bonds when antibonding orbitals are occupied. The IS/HS change in electronic energy is also negative from the change in d-orbital splitting $10Dq$ upon SCO from the $S = 1$ ${}^3T_{1g}$ to the $S = 2$ 5E_g state. The SCO in the 3- NO_2 substituted complex is compared both with the 5- NO_2 substituted and with a complex without any aromatic substituents. According to the calculations, all structures are candidates for a Mn(III) IS to HS SCO.

The B3LYP* and PBE0 functionals give a very consistent picture. The differences in thermal corrections to $\Delta G_{\text{SCO(HS-IS)}}$ are below 1 kJ mol^{-1} for those functionals. B3LYP* gives a slightly larger HS/IS energetic splitting by $\sim 12 \text{ kJ mol}^{-1}$ compared to PBE0. This shows that both functionals are able to correctly describe the $S = 1$ to $S = 2$ spin state change. Spin contamination was not an issue since the $\langle S^2 \rangle$ expectation values were close to the theoretical (2.022 for IS and 6.046 for HS states). The position of the nitro group only has a small effect on the IS/HS state splitting (see Fig. 8). The 3-substituted complex shows the smallest change in Gibbs free energy upon spin transition. For the 5-substituted complex, the spin splitting is larger by a mere 4–5 kJ mol^{-1} . This originates from the electron-withdrawing effect of the NO_2 group, which is more pronounced for the *para*-position.

The overall effect of aromatic nitro substitution becomes most apparent, when comparing with a hypothetical SCO complex without a nitro group which displays the thermodynamically most favorable IS/HS splitting. Introduction of an electron-withdrawing group at either the 3- or 5-position reduces the spin state splitting by 15 and 10 kJ mol^{-1} , respectively. It can be stated that the introduction of an electron-withdrawing group at either the 3- or 5-position only has a minor effect on the spin-state splitting. Whereas most complexes of the *ortho*-series are in the triplet $S = 1$ state, those of the *para*-set are high spin ($S = 2$). The molecular electronic structure can partially rationalize this energetic trend since the IS to HS stabilization becomes less favorable upon *ortho*-substitution.

The calculations reproduce well the structural changes upon spin transition. Here, an effect of the nitro group position is more apparent. For the 3- NO_2 complex, the Mn- N_{amine} distances increase from 2.08 Å to 2.26 and 2.35 Å compared to 2.30 Å when in 5-position. For the Mn- N_{imine} distances, the effect is less pronounced and the distance increases from 1.97 Å to 2.14 and 2.08 Å

TABLE VII. Calculated changes in Gibbs free energies upon triplet (IS) to quintet (HS) spin state transition in kJ mol^{-1} .

			
	3-NO ₂	5-NO ₂	w/o NO ₂
B3LYP*			
ΔE	-17.82	-21.63	-30.70
ΔG_{therm}	-7.58	-8.28	-8.05
$\Delta G_{\text{SCO(HS-IS)}}$	-25.40	-29.91	-38.75
PBE0			
ΔE	-5.95	-10.65	-16.78
ΔG_{therm}	-8.27	-8.89	-9.01
$\Delta G_{\text{SCO(HS-IS)}}$	-14.21	-19.54	-25.79

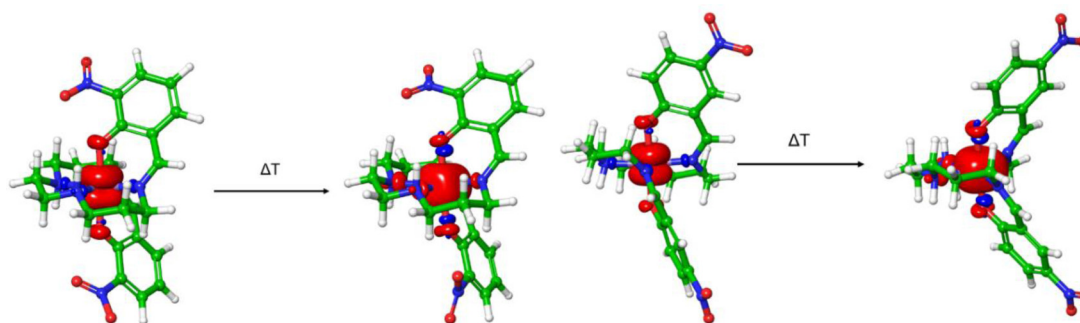
(for NO₂ in 3-position) and from 1.98 to 2.12 Å when in 5-position. In contrast, the Mn-O_{phen} distances are insensitive to the spin state. This shows that the crystallographic Mn-O distances are not a reliable measure to assign an IS or HS state to the complex in the crystal.

2. Influence of the orientation of the substituent

NO₂ is an electron-withdrawing substituent with a preferred orientation in the plane of the aromatic ring. The orientation of the

nitro groups, however, in some of the crystal structures deviates from the strict in-plane orientation. In crystal structures, nitro groups are usually characterized as poor hydrogen bond acceptors and only in a few instances form conventional hydrogen bonds. In particular, this holds for the *para*-substituted complex set (**1b–5b**), which does not reveal significant packing interactions.

For the *ortho*-substitution series (**1a–5a**), however, the nitro groups are neither involved in crystal packing interactions but non-conventional hydrogen bond interactions between equatorial ligand sal C–H and O–NO groups are present (see Fig. 9).

**FIG. 8.** Isocontour plots (at 0.005 e/a.u.) of the unpaired electron spin density for the S = 1 and S = 2 spin states of the Mn(III) complexes with the nitro-substituent in the 3-position (left) and the 5-position (right).

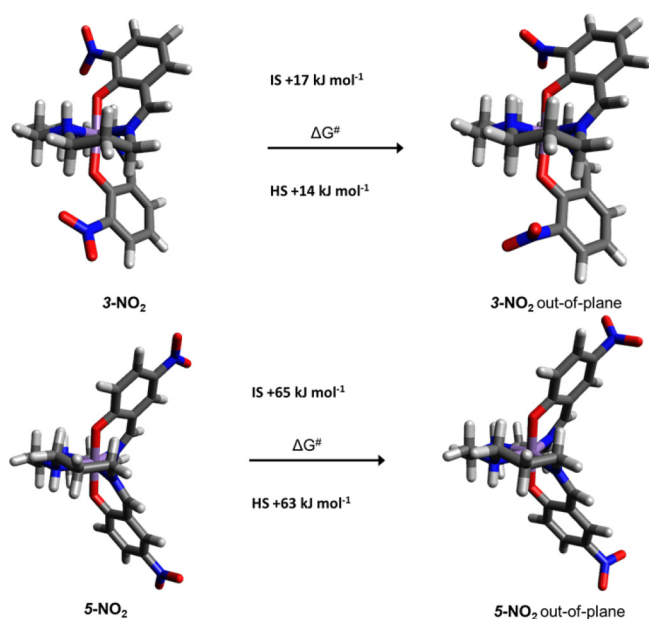


FIG. 9. Calculated transition state barriers of the nitro group rotation in Mn(III) complexes 3- and 5-NO₂ in their intermediate and high-spin states (PBE0/def2-TZVP in kJ mol⁻¹).

Figure 9 shows the changes in Gibbs free energies upon rotating the 3- and 5-NO₂ group from a minimum energy to an out-of-plane orientation. The orientation perpendicular to the aromatic ring is a rotational transition state and characterized by two imaginary frequencies, which correspond to the nitro group out-of-plane rotation. The rotational barrier of the nitro groups is almost independent of the nature of the Mn(III) spin state and corresponds to 65 and 63 kJ mol⁻¹ in 5-NO₂ complexes. The intramolecular stabilization by non-standard C-H...O-NO hydrogen bonds in *ortho*-substituted complexes significantly reduces the rotational barrier from a coplanar to a perpendicular orientation by about 50 kJ mol⁻¹. It should be stressed that the magnitude of electron-withdrawing character of the nitro group is also depending on its conformation. Upon rotation of the nitro group relative to the plane of the benzene ring from 0° to 90°, its electronegativity increases (group electronegativity of the nitro group on the Pauling scale is equal to 4.00 for in-plane and 4.19 for perpendicular orientation),⁴⁸ and this is an additional contribution to the IS to HS transition state splitting. These two factors together explain the different orientations of 3- and 5-nitro groups in the series of Mn(III)-sal crystal structures.

III. CONCLUSIONS

Magnetostructural analysis of two series of Mn(III) complexes from the [Mn(R-sal₂323)]⁺ set of Schiff base complexes, known to facilitate thermal SCO with this ion, has revealed a correlation between spin state preference and position of the electron-withdrawing nitro substituents on the phenolate donors. With the *ortho*-

substituted Schiff base ligand, 3-NO₂-sal₂-323, the tendency is toward stabilization of the *S* = 1 spin state in complexes (1a)–(5a), in contrast to stabilization of the *S* = 2 state with the *para*-substituted Schiff base analog 5-NO₂-sal₂-323 in (1b)–(5b). The difference in spin state preferences could be correlated with the difference in twist angles of the nitro groups, which in turn was related to the ease of forming short contacts with adjacent hydrogen atoms. The nitro groups in the complexes with the *ortho*-substituted ligands (1a)–(5a) were found to be flipped out-of-plane of the phenolate ring in contrast to the corresponding twist angles of the nitro groups in the *para* position which were largely in-plane with the phenolate rings in complexes (1b)–(5b). The out-of-plane deformation can be explained by non-classical CH...ON hydrogen bond interactions and an orientation-dependent electronegativity of the nitro group. Potential thermal structural phase transitions were detected in three of the complexes with the *ortho*-substituted ligands which will be investigated more fully by single crystal diffraction at multiple temperatures. In addition, one complex with the *para*-substituted ligand broke the trend for the orientation of the Jahn–Teller distortion typical for HS complexes with this ligand type in that an elongation in the N₄O₂ plane, rather than the expected N₄ plane, was observed in complex (1b). The Mn(III) octahedral complexes (1)–(5) display a large variety of magnetic behavior. Although chemically identical, their solid-state properties can be tuned by variation of counterions and/or co-crystallized solvent. Computational methods are now able to accurately calculate the energetics of splitting of different spin states. Thus, it may be possible to also suggest novel complexes with SCO based on a computational fine-tuning of ligand fields. Their performance in the crystalline state, however, cannot be predicted since it is the cooperativity of a multitude of parameters that need to come together to enable the SCO.

IV. MATERIALS AND METHODS

A. Materials and physical measurements

All chemicals and solvents if not otherwise mentioned were purchased from chemical companies and were reagent grade. They were used without further purification or drying. All reactions were carried out under ambient conditions. All measurements were carried out on powdered samples of the respective polycrystalline compound which in some cases were fitted with partial solvation according to CHN data on the bulk sample. Elemental analysis (C, H, and N) were performed using a Perkin Elmer Vario EL. A Bruker Alpha PlatinumATIR spectrometer, was used to record the infrared spectra, and mass spectra were recorded on a Waters 2695 Separations Module Electrospray Spectrometer.

B. Synthesis and characterization of compounds

[Mn(L1)]NO₃ (1a): [Mn(L₁)]NO₃: 2.0 mmol 2-hydroxy-3-nitrobenzaldehyde (0.334 g) was dissolved in 10.0 ml ethanol/acetone (50:50 v:v) and stirred for 10 min at room temperature. 1.0 mmol 1,2-bis(3-aminopropylamino)ethane (0.165 ml) was added and the color started to change immediately. 1.0 mmol Mn(NO₃)₂·6H₂O (0.361 g) was dissolved in ethanol (10 ml), filtered, and added to the stirring ligand solution. Upon

complexation, a color change from yellow to dark red/brown was observed. The reaction mixture was stirred for further 3 h. The dark red solution was then filtered and left standing for slow evaporation, which yielded dark red/black crystals of complex **1a** which were suitable for single crystal x-ray analysis.

Elemental analysis for $[\text{C}_{22}\text{H}_{26}\text{N}_7\text{O}_9\text{Mn}]$: calculated: C: 44.98, H: 4.46, N: 16.69; found: 44.81, H: 4.58, N: 16.72.

[Mn(L1)]ClO₄ (2a): Complex **2a** was synthesized following the procedure for complex **1a** where $\text{Mn}(\text{NO}_3)_2 \cdot 6\text{H}_2\text{O}$ was replaced with 1.0 mmol $\text{Mn}(\text{ClO}_4)_2 \cdot 6\text{H}_2\text{O}$.

Elemental analysis for $[\text{C}_{22}\text{H}_{26}\text{N}_6\text{O}_{10}\text{ClMn}]$: calculated: C: 42.29, H: 4.19, N: 13.45; found: 42.20, H: 4.12, N: 13.33.

[Mn(L1)]PF₆ (3a): Complex **3a** was synthesized following the procedure for complex **1a** where $\text{Mn}(\text{NO}_3)_2 \cdot 6\text{H}_2\text{O}$ was replaced with 1.0 mmol $\text{MnCl}_2 \cdot 4\text{H}_2\text{O}$ (0.197 g) and 1.0 mmol NH_4PF_6 (0.163 g).

Elemental analysis for $[\text{C}_{22}\text{H}_{26}\text{F}_6\text{N}_6\text{O}_6\text{PMn}] \cdot 0.15\text{H}_2\text{O}$: calculated: C: 39.77, H: 3.97, N: 12.31; found: C: 39.86, H: 4.32, N: 12.65.

[Mn(L1)]OTf (4a): Complex **4a** was synthesized following the procedure for complex **1a** where $\text{Mn}(\text{NO}_3)_2 \cdot 6\text{H}_2\text{O}$ was replaced with 1.0 mmol $\text{MnCl}_2 \cdot 4\text{H}_2\text{O}$ (0.197 g) and 1.0 mmol AgCF_3SO_3 (0.257 g).

Elemental analysis for $[\text{C}_{23}\text{H}_{26}\text{N}_6\text{O}_9\text{F}_3\text{SMn}]$: calculated: C: 40.36, H: 3.89, N: 12.46; found: C: 39.90, H: 3.50, N: 12.86.

[Mn(L1)]BPh₄·2MeCN and [Mn(L1)]BPh₄·3MeCN (5a): Complex **5a** was synthesized following the procedure for complex **1a** where $\text{Mn}(\text{NO}_3)_2 \cdot 6\text{H}_2\text{O}$ was replaced with 1.0 mmol $\text{MnCl}_2 \cdot 4\text{H}_2\text{O}$ (0.197 g) and 1.0 mmol NaBPh_4 (0.343 g).

Elemental analysis for dried sample of **5b·2MeCN**: $[\text{C}_{50}\text{H}_{52}\text{BN}_8\text{O}_6\text{Mn}]$ (solv free): calculated: C: 65.41, H: 5.49, N: 9.95; found: C: 65.36, H: 5.85, N: 10.24. (Fit with partial solvation: $[\text{C}_{50}\text{H}_{52}\text{BN}_8\text{O}_6\text{Mn}] \cdot 0.45\text{MeCN} \cdot 0.15\text{H}_2\text{O}$: calculated: C: 65.06, H: 5.55, N: 10.43; found: C: 65.36, H: 5.85, N: 10.24).

Elemental analysis for dried sample of **5b·3MeCN**: $[\text{Mn}(\text{L1})\text{BPh}_4 \cdot 2.1\text{MeCN} \cdot 0.85\text{H}_2\text{O}]$: calculated: 63.72, H: 5.75, N: 11.99; found: C: 63.50, H: 5.52, N: 12.16.

[Mn(L2)]NO₃·1MeCN·0.5H₂O (1b): A solution of 5-nitrosalicylaldehyde (0.334 g, 2 mmol) dissolved in ethanol/acetonitrile (50:50 v:v 10 ml) was added to a well stirred solution of *N,N'*-bis-(3-aminopropyl)ethylenediamine (0.174 g, 1 mmol) in ethanol/acetonitrile (50:50 v:v 10 ml), by gravity filtration. When Schiff base formation, indicated by the intense yellow color, was achieved, a solution of manganese(II) nitrate hexahydrate (0.287 g, 1 mmol) ethanol/acetonitrile (50:50 v:v 10 ml), was added dropwise resulting in a dark brown solution which was stirred for 3 h before gravity filtration and standing in air which yielded crystals of x-ray quality.

Elemental analysis for $[\text{C}_{48}\text{H}_{60}\text{N}_{16}\text{O}_{19}\text{Mn}_2] \cdot \text{MeCN} \cdot 0.5\text{H}_2\text{O}$: calculated: C: 45.22, H: 4.74, N: 17.58; found: C: 45.05, H: 4.55, N: 17.30.

[Mn(L2)]ClO₄·0.5MeCN·0.5H₂O (2b): Complex **2b** was synthesized following the procedure for complex **1b** where $\text{Mn}(\text{NO}_3)_2 \cdot 6\text{H}_2\text{O}$ was replaced with 1.0 mmol $\text{Mn}(\text{ClO}_4)_2 \cdot 6\text{H}_2\text{O}$.

Elemental analysis for $[\text{C}_{22}\text{H}_{26}\text{N}_6\text{O}_{10}\text{ClMn}] \cdot 0.4\text{MeCN} \cdot 1.2\text{H}_2\text{O}$: calculated: C: 41.31, H: 4.50, N: 13.52; found: C: 41.18, H: 4.37, N: 13.63.

[Mn(L2)]PF₆ (3b): Complex **3b** was synthesized following the procedure for complex **1b** where $\text{Mn}(\text{NO}_3)_2 \cdot 6\text{H}_2\text{O}$ was replaced with 1.0 mmol $\text{MnCl}_2 \cdot 4\text{H}_2\text{O}$ (0.197 g) and 1.0 mmol NH_4PF_6 (0.163 g).

Elemental analysis for $[\text{C}_{22}\text{H}_{26}\text{N}_6\text{O}_6\text{F}_6\text{PMn}] \cdot 0.15\text{H}_2\text{O} \cdot 0.1\text{EtOH}$: calculated: C: 39.77, H: 3.97, N: 12.31; found: C: 39.86, H: 3.97, N: 12.31.

[Mn(L2)]OTf (4b): Complex **4b** was synthesized following the procedure for complex **1b** where $\text{Mn}(\text{NO}_3)_2 \cdot 6\text{H}_2\text{O}$ was replaced with 1.0 mmol $\text{MnCl}_2 \cdot 4\text{H}_2\text{O}$ (0.197 g) and 1.0 mmol AgCF_3SO_3 (0.257 g).

Elemental analysis for $[\text{C}_{23}\text{H}_{26}\text{N}_6\text{O}_9\text{F}_3\text{SMn}]$: calculated: C: 40.96, H: 3.89, N: 12.46; found: C: 41.14, H: 3.99, N: 12.82.

[Mn(L2)]BPh₄ (5b): Complex **5b** was synthesized following the procedure for complex **1b** where $\text{Mn}(\text{NO}_3)_2 \cdot 6\text{H}_2\text{O}$ was replaced with 1.0 mmol $\text{MnCl}_2 \cdot 4\text{H}_2\text{O}$ (0.197 g) and 1.0 mmol NaBPh_4 (0.343 g).

Elemental analysis for $[\text{C}_{46}\text{H}_{46}\text{BN}_6\text{O}_6\text{Mn}] \cdot 2.3\text{H}_2\text{O}$: calculated: C: 62.35, H: 5.76, N: 9.48; found: C: 62.25, H: 5.64, N: 9.49.

C. Single-crystal x-ray structure determination

Suitable single crystals of complexes (1)–(5) were mounted on an Oxford Diffraction Supernova A diffractometer fitted with an Atlas detector; datasets were measured using monochromatic Cu-K α radiation or Mo-K α radiation and corrected for absorption.⁴⁹ The temperatures were controlled with an Oxford Instruments' Cryojet. Structures were solved by direct methods (SHELXS) and refined with full-matrix least-squared procedures based on F^2 , using SHELXL-1997 or -2016.⁵⁰ Non-hydrogen atoms were refined with independent anisotropic displacement parameters, organic H-atoms (i.e., bonded to C) were placed in idealized positions, while the coordinates of H-atoms bonded to O were generally refined with their O-H distance restrained to 0.84 Å; details are described in the cif for each structure. In general, if disorder had to be modeled, the sum of the site occupation factors was con- or restrained to be 1. In the 100 K structure of $[\text{MnL}_1]\text{PF}_6$ (**3a**), the oxygen atom O5 of the NO₂ substituent of the Schiff base ligand displays a disorder over two positions with site occupation factors 0.492 (8) and 0.508(2). The 100 K structure of $[\text{MnL}_1]\text{OTf}$ (**4a**) shows a similar disorder of one nitro group of the Schiff base ligand but this time both oxygen atoms, O10 and O11, are displaced over two positions with site occupation factors of 0.619(5) for O10A and O11A and 0.381(5) for O10B and O11B. The disorder within one of the triflate anions was modeled over two sites with site occupation factors 0.555(3) and 0.445(3). The 200 K structure of **5a·2MeCN** exhibits a disorder of one nitro group of the Schiff base ligand over both oxygen atoms, O4 and O5, which are displaced over two positions with site occupation factors of 0.45(2) for O4A and O5A and 0.55(2) for O4B and O5B. The perchlorate anions within the crystal lattice of **2b·0.5MeCN·0.5H₂O** exhibit a high degree of disorder and were modeled with site occupation factors fixed to 0.5 and 0.25, respectively. One of the two hexafluorophosphate anions within (**3b**) at 100 K exhibits a disorder of four of its equatorially surrounding fluorine atoms over three possible sites with site occupation factors of 0.431(8), 0.357(8), and 0.212(5). Selected crystallographic data and structure refinements are summarized in Tables S1-S5 in the [supplementary material](#).

D. Magnetic measurements

The magnetic susceptibility measurements were recorded on a Quantum Design SQUID magnetometer MPMS-XL operating

between 5 and 300 K. DC measurements were performed on polycrystalline samples. Each sample was wrapped in a gelatine capsule and subjected to fields of 0.5 T. Diamagnetic corrections were applied to correct for contribution from the sample holder, and the inherent diamagnetism of the sample was estimated with the use of Pascal's constants.

E. Computational details

All calculations were performed with Turbomole 7.5.^{51,52} The calculations largely follow the protocol outlined in Refs. 53 and 27. The triplet and quintet states were structurally minimized at the BP86 level using a def2-SVP basis set.⁵⁴ The COSMO implicit solvation model ($\epsilon = 80$)⁵⁵ was employed in order to account for environmental effects on the charged molecular structures.⁵⁶ This choice of functional and basis reproduce structures of transition metal complexes very well. Analytical frequencies were calculated at the BP86/def2-SVP level in order to obtain zero point vibrational energies (ZPVEs) and thermodynamic corrections ΔG_{therm} . Since the focus here is on energy differences between intermediate and high-spin states, the differences are only weakly affected by scaling, basis set, or functional. Subsequent single point energies used the larger def2-TZVPP basis set were calculated with the hybrid functionals B3LYP^{57–59} with 20% Hartree–Fock exchange and the B3LYP* with 15% Hartree–Fock exchange.^{60,61} The reduction in exchange was shown to be essential for the description of spin-crossover complexes.^{62–64} Dispersion effects were considered using the D3 correction with Becke–Johnson damping,^{65,66} which are critical for the description of energies. For reasons of consistency, PBE0-D3(BJ) (with 25% HF exchange) geometry optimizations and frequency calculations with a def2-TZVP basis set were augmented by PBE0-D3(BJ)/def2-TZVPP single point calculations.⁶⁷

SUPPLEMENTARY MATERIAL

See the [supplementary material](#) for the crystallographic data tables for all compounds and views of the intramolecular interactions for selected example references within the main text.

ACKNOWLEDGMENTS

We thank SFI for generous support via Frontiers for the Future Award (No. 19/FFP/6909 to G.G.M). This research was also supported by a Government of Ireland Research Scholarship from the Irish Research Council for Science Engineering and Technology (B.G.) as well as an Irish Research Council GOIPD/2016/503 Postdoctoral Fellowship (I.A.K.), the award of a National University of Ireland Travelling Scholarship (M.H.), and a post-graduate studentship from University College Dublin and Meath County Council (L.C.G.). We acknowledge the EU COST Actions CA15128 Molecular Spintronics (MOLSPIN), CM1305, Explicit Control over Spin-states in Technology and Biochemistry, (ECOSTBio), and CA15107 Multi-Functional Nano-Carbon Composite Materials Network (MultiComp). M.S. is grateful to the Max Planck Society for the Advancement of Science for financial support.

DATA AVAILABILITY

Crystallographic data for the structures reported in this paper are openly available in Cambridge Crystallographic Data Centre (CCDC) as supplementary publication Nos. CCDC-2056235-2056255, <https://www.ccdc.cam.ac.uk/structures/>. The data that support the findings of this study are available from the corresponding author upon reasonable request.

REFERENCES

- ¹Halcrow, M. A. in *Spin-Crossover Materials*, edited by M. A. Halcrow (John Wiley & Sons Ltd., Oxford, 2013). ISBN 9781118519301.
- ²K. S. Kumar and M. Ruben, "Sublimable spin-crossover complexes: From spin-state switching to molecular devices," *Angew. Chem. Int. Ed.* **60**, 7502–7521 (2021).
- ³M. Estrader, J. Salinas Uber, L. A. Barrios, J. Garcia, P. Lloyd-Williams, O. Roubeau, S. J. Teat, and G. Aromí, "A magneto-optical molecular device: Interplay of spin crossover, luminescence, photomagnetism, and photochromism," *Angew. Chem. Int. Ed.* **56**, 15622–15627 (2017).
- ⁴X. Zhang, T. Palamarciuc, J.-F. Létard, P. Rosa, E. V. Lozada, F. Torres, L. G. Rosa, B. Doudin, and P. A. Dowben, "The spin state of a molecular adsorbate driven by the ferroelectric substrate polarization," *Chem. Commun.* **50**, 2255 (2014).
- ⁵Y. Otsuki, S. Kimura, S. Awaji, and M. Nakano, "Magneto-capacitance effect and magnetostriction by the field-induced spin-crossover in [MnIII(taa)]," *AIP Adv.* **9**, 085219 (2019).
- ⁶S.-I. Ohkoshi, K. Imoto, Y. Tsunobuchi, S. Takano, and H. Tokoro, "Light-induced spin-crossover magnet," *Nat. Chem.* **3**, 564–569 (2011).
- ⁷S. Dhers, A. Mondal, D. Aguilà, J. Ramirez, S. Vela, P. Dechambenoit, M. Rouzières, J. R. Nitschke, R. Clérac, and J.-M. Lehn, "Spin state chemistry: Modulation of ligand pKa by spin state switching in a [2x2] iron(II) grid-type complex," *J. Am. Chem. Soc.* **140**, 8218–8227 (2018).
- ⁸M. van Veenendaal, "Time-dependent nonequilibrium soft x-ray response during a spin crossover," *Phys. Rev. B* **97**, 125108 (2018).
- ⁹S. T. Park and R. M. van der Veen, "Modeling nonequilibrium dynamics of phase transitions at the nanoscale: Application to spin-crossover," *Struct. Dyn.* **4**, 044028 (2017).
- ¹⁰J. M. Herrera, S. Titos-Padilla, S. J. A. Pope, I. Berlanga, F. Zamora, J. J. Delgado, K. V. Kamenev, X. Wang, A. Prescimone, E. K. Brechin *et al.*, "Studies on bifunctional Fe(II)-triazole spin crossover nanoparticles: Time-dependent luminescence, surface grafting and the effect of a silica shell and hydrostatic pressure on the magnetic properties," *J. Mater. Chem. C* **3**, 7819–7829 (2015).
- ¹¹T. Mallah and M. Cavallini, "Surfaces, thin films and patterning of spin crossover compounds," *CR Chim.* **21**, 1270–1286 (2018).
- ¹²A. Bousseksou, G. Molnár, L. Salmon, and W. Nicolazzi, "Molecular spin crossover phenomenon: Recent achievements and prospects," *Chem. Soc. Rev.* **40**, 3313 (2011).
- ¹³K. Senthil Kumar and M. Ruben, "Emerging trends in spin crossover (SCO) based functional materials and devices," *Coord. Chem. Rev.* **346**, 176–205 (2017).
- ¹⁴K. Ridier, A.-C. Bas, Y. Zhang, L. Routaboul, L. Salmon, G. Molnár, C. Bergaud, and A. Bousseksou, "Unprecedented switching endurance affords for high-resolution surface temperature mapping using a spin-crossover film," *Nat. Commun.* **11**, 3611 (2020).
- ¹⁵M. Hostettler, K. W. Törnroos, D. Chernyshov, B. Vangdal, and H.-B. Bürgi, "Challenges in engineering spin crossover: Structures and magnetic properties of six alcohol solvates of iron(II) tris(2-picolylamine) dichloride," *Angew. Chem. Int. Ed.* **43**, 4589–4594 (2004).
- ¹⁶Z. Arcis-Castillo, S. Zheng, M. A. Siegler, O. Roubeau, S. Bedoui, and S. Bonnet, "Tuning the transition temperature and cooperativity of babbpy-based

mononuclear spin-crossover compounds: Interplay between molecular and crystal engineering," *Chem. Eur. J.* **17**, 14826–14836 (2011).

¹⁷Y. Garcia, N. N. Adarsh, and A. D. Naik, "Crystal engineering of FeII spin crossover coordination polymers derived from triazole or tetrazole ligands," *Chim. Int. J. Chem.* **67**, 411–418 (2013).

¹⁸M. A. Halcrow, "Structure: function relationships in molecular spin-crossover complexes," *Chem. Soc. Rev.* **40**, 4119 (2011).

¹⁹L. J. Kershaw Cook, R. Kulmaczewski, R. Mohammed, S. Dudley, S. A. Barrett, M. A. Little, R. J. Deeth, and M. A. Halcrow, "A unified treatment of the relationship between ligand substituents and spin state in a family of iron(II) complexes," *Angew. Chem. Int. Ed.* **55**, 4327–4331 (2016).

²⁰M. Halcrow, "The effect of ligand design on metal ion spin state—Lessons from spin crossover complexes," *Crystals* **6**, 58 (2016).

²¹C. J. Johnson, G. G. Morgan, and M. Albrecht, "Predictable adjustment of spin crossover temperature in solutions of iron(III) complexes functionalized with alkyl-urea tails," *J. Mater. Chem. C* **3**, 7883–7889 (2015).

²²S. Sundaresan, J. A. Kitchen, and S. Brooker, "Hydrophobic tail length in spin crossover active iron(II) complexes predictably tunes $T_{1/2}$ in solution and enables surface immobilisation," *Inorg. Chem. Front.* **7**, 2050–2059 (2020).

²³J. Olguín, "Unusual metal centres/coordination spheres in spin crossover compounds," *Coord. Chem. Rev.* **407**, 213148 (2020).

²⁴K. Pandurangan, B. Gildea, C. Murray, C. J. Harding, H. Müller-Bunz, and G. G. Morgan, "Lattice effects on the spin-crossover profile of a mononuclear manganese(III) cation," *Chem. Eur. J.* **18**, 2021–2029 (2012).

²⁵B. Gildea, M. M. Harris, L. C. Gavin, C. A. Murray, Y. Ortin, H. Müller-Bunz, C. J. Harding, Y. Lan, A. K. Powell, and G. G. Morgan, "Substituent effects on spin state in a series of mononuclear manganese(III) complexes with hexadentate Schiff-base ligands," *Inorg. Chem.* **53**, 6022–6033 (2014).

²⁶B. Gildea, L. C. Gavin, C. A. Murray, H. Müller-Bunz, C. J. Harding, and G. G. Morgan, "Supramolecular modulation of spin crossover profile in manganese(III)," *Supramol. Chem.* **24**, 641–653 (2012).

²⁷I. A. Kühne, A. Barker, F. Zhang, P. Stamenov, O. O'Doherty, H. Müller-Bunz, M. Stein, B. J. Rodriguez, and G. G. Morgan, "Modulation of Jahn–Teller distortion and electromechanical response in a Mn^{3+} spin crossover complex," *J. Phys.: Condens. Matter* **32**, 404002 (2020).

²⁸I. A. Kühne, K. Esien, L. C. Gavin, H. Müller-Bunz, S. Felton, and G. G. Morgan, "Modulation of Mn^{3+} spin state by guest molecule inclusion," *Molecules* **25**, 5603 (2020).

²⁹G. G. Morgan, K. D. Murnaghan, H. Müller-Bunz, V. McKee, and C. J. Harding, "A manganese(III) complex that exhibits spin crossover triggered by geometric tuning," *Angew. Chem. Int. Ed.* **45**, 7192–7195 (2006).

³⁰A. J. Fitzpatrick, E. Trzop, H. Müller-Bunz, M. M. Dirtu, Y. Garcia, E. Collet, and G. G. Morgan, "Electronic vs structural ordering in a manganese(III) spin crossover complex," *Chem. Commun.* **51**, 17540–17543 (2015).

³¹P. N. Martinho, B. Gildea, M. M. Harris, T. Lemma, A. D. Naik, H. Müller-Bunz, T. E. Keyes, Y. Garcia, and G. G. Morgan, "Cooperative spin transition in a mononuclear manganese(III) complex," *Angew. Chem. Int. Ed.* **51**, 12597–12601 (2012).

³²A. Barker, C. T. Kelly, I. A. Kühne, S. Hill, J. Krzystek, P. Wix, K. Esien, S. Felton, H. Müller-Bunz, and G. G. Morgan, "Spin state solvomorphism in a series of rare $S = 1$ manganese(III) complexes," *Dalton Trans.* **48**, 15560–15566 (2019).

³³V. B. Jakobsen, E. Trzop, L. C. Gavin, E. Dobbelaar, S. Chikara, X. Ding, K. Esien, H. Müller-Bunz, S. Felton, V. S. Zapf *et al.*, "Stress-induced domain wall motion in a ferroelastic Mn^{3+} spin crossover complex," *Angew. Chem. Int. Ed.* **59**, 13305–13312 (2020).

³⁴V. B. Jakobsen, L. O'Brien, G. Novitchi, H. Müller-Bunz, A.-L. Barra, and G. G. Morgan, "Chiral resolution of a Mn^{3+} spin crossover complex," *Eur. J. Inorg. Chem.* **2019**, 4405–4411 (2019).

³⁵V. B. Jakobsen, S. Chikara, J.-X. Yu, E. Dobbelaar, C. T. Kelly, X. Ding, F. Weickert, E. Trzop, E. Collet, H.-P. Cheng *et al.*, "Giant magnetoelectric coupling and magnetic-field-induced permanent switching in a spin crossover Mn(III) complex," *Inorg. Chem.* **60**, 6167 (2021).

³⁶J. Sirirak, D. J. Harding, P. Harding, K. S. Murray, B. Moubarak, L. Liu, and S. G. Telfer, "Spin crossover in cis manganese(III) quinolylsalicylaldehydes," *Eur. J. Inorg. Chem.* **2015**, 2534–2542.

³⁷M. S. Shongwe, K. S. Al-Barhi, M. Mikuriya, H. Adams, M. J. Morris, E. Bill, and K. C. Molloy, "Tuning a single ligand system to stabilize multiple spin states of manganese: A first example of a hydrazone-based manganese(III) spin-crossover complex," *Chem. Eur. J.* **20**, 9693–9701 (2014).

³⁸Z. Liu, S. Liang, X. Di, and J. Zhang, "A manganese(III) complex that exhibits spin crossover behavior," *Inorg. Chem. Commun.* **11**, 783–786 (2008).

³⁹H. Paulsen and A. X. Trautwein, "Density functional theory calculations for spin crossover complexes," in *Spin Crossover in Transition Metal Compounds III*, edited by P. Gtlich and H. A. Goodwin, (Springer-Verlag, Berlin), pp. 197–219. (2004)

⁴⁰K. P. Kepp, "Consistent descriptions of metal–ligand bonds and spin-crossover in inorganic chemistry," *Coord. Chem. Rev.* **257**, 196–209 (2013).

⁴¹H. Paulsen, V. Schünemann, and J. A. Wolny, "Progress in electronic structure calculations on spin-crossover complexes," *Eur. J. Inorg. Chem.* **2013**, 628–641 (2013).

⁴²S. Ye and F. Neese, "Accurate modeling of spin-state energetics in spin-crossover systems with modern density functional theory," *Inorg. Chem.* **49**, 772–774 (2010).

⁴³M. Radoń, "Benchmarking quantum chemistry methods for spin-state energetics of iron complexes against quantitative experimental data," *Phys. Chem. Chem. Phys.* **21**, 4854–4870 (2019).

⁴⁴J. Cirera, M. Via-Nadal, and E. Ruiz, "Benchmarking density functional methods for calculation of state energies of first Row spin-crossover molecules," *Inorg. Chem.* **57**, 14097–14105 (2018).

⁴⁵S. Amabilino and R. J. Deeth, "DFT analysis of spin crossover in Mn(III) complexes: Is a two-electron $S = 2$ to $S = 0$ spin transition feasible?," *Inorg. Chem.* **56**, 2602–2613 (2017).

⁴⁶M. G. B. Drew, C. J. Harding, V. McKee, G. G. Morgan, and J. Nelson, "Geometric control of manganese redox state," *J. Chem. Soc. Chem. Commun.* **10**, 1035 (1995).

⁴⁷R. Ketkaew, Y. Tantirungrotechai, P. Harding, G. Chastanet, P. Guionneau, M. Marchivie, and D. J. Harding, "Octadist: A tool for calculating distortion parameters in spin crossover and coordination complexes," *Dalton Trans.* **50**, 1086–1096 (2021).

⁴⁸A. R. Campanelli, A. Domenicano, F. Ramondo, and I. Hargittai, "Group electronegativities from benzene ring deformations: A quantum chemical study," *J. Phys. Chem. A* **108**, 4940–4948 (2004).

⁴⁹R. C. Clark and J. S. Reid, "The analytical calculation of absorption in multi-faceted crystals," *Acta Crystallogr. Sect. A* **51**, 887–897 (1995).

⁵⁰G. M. Sheldrick, "Crystal structure refinement with SHELXL," *Acta Crystallogr. Sect. C Struct. Chem.* **71**, 3–8 (2015).

⁵¹S. G. Balasubramani, G. P. Chen, S. Coriani, M. Diedenhofen, M. S. Frank, Y. J. Franzke, F. Furche, R. Grotjahn, M. E. Harding, C. Hättig *et al.*, "TURBOMOLE: Modular program suite for *ab initio* quantum-chemical and condensed-matter simulations," *J. Chem. Phys.* **152**, 184107 (2020).

⁵²TURBOMOLE V7.5 2020, a development of University of Karlsruhe and Forschungszentrum Karlsruhe GmbH, 1989–2007; TURBOMOLE GmbH, since 2007; available at <https://www.turbomole.org>.

⁵³K. P. Kepp, "Theoretical study of spin crossover in 30 iron complexes," *Inorg. Chem.* **55**, 2717–2727 (2016).

⁵⁴F. Weigend and R. Ahlrichs, "Balanced basis sets of split valence, triple zeta valence and quadruple zeta valence quality for H to Rn: Design and assessment of accuracy," *Phys. Chem. Chem. Phys.* **7**, 3297 (2005).

⁵⁵A. Klamt and G. Schüürmann, "COSMO: A new approach to dielectric screening in solvents with explicit expressions for the screening energy and its gradient," *J. Chem. Soc., Perkin Trans. 2*, 799–805 (1993).

⁵⁶K. P. Jensen and M. Rykær, "The building blocks of metallothioneins: Heterometallic Zn^{2+} and Cd^{2+} clusters from first-principles calculations," *Dalton Trans.* **39**, 9684 (2010).

⁵⁷P. J. Stephens, F. J. Devlin, C. F. Chabalowski, and M. J. Frisch, "*Ab initio* calculation of vibrational absorption and circular dichroism spectra using density functional force fields," *J. Phys. Chem.* **98**, 11623–11627 (1994).

- ⁵⁸C. Lee, W. Yang, and R. G. Parr, "Development of the Colle-Salvetti correlation-energy formula into a functional of the electron density," *Phys. Rev. B* **37**, 785–789 (1988).
- ⁵⁹A. D. Becke, "Density-functional thermochemistry. III. The role of exact exchange," *J. Chem. Phys.* **98**, 5648–5652 (1993).
- ⁶⁰M. Reiher, O. Salomon, and B. Artur Hess, "Reparameterization of hybrid functionals based on energy differences of states of different multiplicity," *Theor. Chem. Acc.* **107**, 48–55 (2001).
- ⁶¹O. Salomon, M. Reiher, and B. A. Hess, "Assertion and validation of the performance of the B3LYP* functional for the first transition metal row and the G2 test set," *J. Chem. Phys.* **117**, 4729–4737 (2002).
- ⁶²M. Reiher, "Theoretical study of the Fe(phen)₂(NCS)₂ spin-crossover complex with reparametrized density functionals," *Inorg. Chem.* **41**, 6928–6935 (2002).
- ⁶³M. Bruschi, L. De Gioia, G. Zampella, M. Reiher, P. Fantucci, and M. Stein, "A theoretical study of spin states in Ni-S4 complexes and models of the [NiFe] hydrogenase active site," *JBIC J. Biol. Inorg. Chem.* **9**, 873–884 (2004).
- ⁶⁴E. Edler and M. Stein, "Spin-state-dependent properties of an iron(III) hydrogenase mimic," *Eur. J. Inorg. Chem.* **2014**, 3587–3599 (2014).
- ⁶⁵S. Grimme, J. Antony, S. Ehrlich, and H. Krieg, "A consistent and accurate *ab initio* parametrization of density functional dispersion correction (DFT-D) for the 94 elements H-Pu," *J. Chem. Phys.* **132**, 154104 (2010).
- ⁶⁶S. Grimme, S. Ehrlich, and L. Goerigk, "Effect of the damping function in dispersion corrected density functional theory," *J. Comput. Chem.* **32**, 1456–1465 (2011).
- ⁶⁷C. Adamo and V. Barone, "Toward reliable density functional methods without adjustable parameters: The PBE0 model," *J. Chem. Phys.* **110**, 6158–6170 (1999).